Petrogenesis and thermobarometry of the ~50 Ma rapakivi granite-syenite Acapulco intrusive: Implications for post-Laramide magmatism in southern Mexico

Guillermo A. Hernández-Pineda[1,*], Luigi A. Solari[2], Arturo Gómez-Tuena[2], Doris L. Méndez-Cárdenas[3], and Ofelia Pérez-Arvizu[2]

[1]*Instituto de Geología, Universidad Nacional Autónoma de México, Ciudad Universitaria, 04510 México, D.F., Mexico*
[2]*Centro de Geociencias, Universidad Nacional Autónoma de México, Campus Juriquilla, 76001 Querétaro, QRO, Mexico*
[3]*Instituto de Geofísica, Universidad Nacional Autónoma de México, Ciudad Universitaria, 04510 México, D.F., Mexico*

ABSTRACT

The Acapulco intrusion is a composite pluton that belongs to the coastal batholithic belt of southern Mexico, intruding the Xolapa metamorphic complex and cropping out in the neighboring area of Acapulco city. The Acapulco intrusion has been considered as an anomaly based on its age, which contrasts with the surrounding plutons and the general age trend from the coastal batholithic belt and corresponds to an Eocene–Oligocene age. It ranges in composition from granite (sensu stricto) to syenite and diorite. The most distinctive characteristic of the Acapulco intrusion is the rapakivi texture developed in the granites, which are characterized by biotite, amphibole, allanite, and fluorite as distinctive minerals, plus titanite, zircon, and apatite as accessory phases.

Geochemically, the Acapulco intrusion varies from metaluminous to peraluminous, and displays the distinctive signatures of arc-related magmas. The studied rocks show strong negative Sr, Ba, and Eu anomalies, coupled with incompatible element enrichments and high Ga/Al ratios, which are typical characteristics of A-type granites that underwent strong plagioclase fractionation from a formerly metaluminous magma.

Initial isotopic ratios ($^{87}Sr/^{86}Sr$ from 0.7035 to 0.7100, and εNd from +5.50 to +1.78) indicate a range from depleted mantle compositions to compositions consistent with crustal contamination by continental crust, particularly from the surrounding Xolapa Complex. U-Pb geochronology in zircons by laser ablation–inductively coupled plasma–mass spectrometry (LA-ICP-MS) established crystallization ages of 49.40 ± 0.40 Ma, 50.20 ± 1.0 Ma, 50.42 ± 0.39 Ma, and 50.56 ± 0.39 Ma for different lithologies of the Acapulco intrusion. These geochronological data, together with previous published works, confirm that post-Laramide plutonism between 50 and 60 Ma is widespread in the southern continental margin of Mexico as a major magmatic event.

Finally, new thermobarometric determinations established emplacement conditions of ~700 °C at 8–10 km depth (2.08–2.8 kbar), indicating an exhumation rate of ~0.21 km/m.y. between 50 and 20 Ma, which is slower than the previous estimated rate of 0.44 km/m.y. These results call for a review on models suggesting fast and/or slow exhumation of the southern Mexico coastal batholitic belt.

INTRODUCTION

The active continental margin in southwestern Mexico has been continuously evolving at least since the Jurassic as a result of the eastward subduction of the Pacific-Farallón-Cocos and Rivera plates under the continental crust of the North American plate (e.g., Ortega-Gutiérrez et al., 1994; Dickinson and Lawton, 2001; Morán-Zenteno et al., 2007). Whereas the post-Eocene, subduction-related magmatism is exposed as a volcanic arc (e.g., Martiny et al., 2000; Morán-Zenteno et al., 2007), its plutonic counterpart for the Mesozoic and early Tertiary is mainly exposed along the Pacific coast (Morán-Zenteno et al., 1999). This belt, which broadly extends from Puerto Vallarta to Huatulco, is known as the coastal batholithic belt (Schaaf et al., 1995; Morán-Zenteno et al., 1999, 2005; Martiny et al., 2000; Solari et al., 2007; Martini et al., 2009; Pérez-Gutiérrez et al., 2009). The tectonic evolution of the plutonic belt of southwestern Mexico broadly corresponds with the Laramide orogeny of the western Cordillera in North America and Canada. Locally it has been associated with terrane accretion (e.g., Campa and Coney, 1983; Talavera-Mendoza et al., 2007) or shearing during eastward arc migration (e.g., Martini et al., 2009), combined with shear transmission between lower and upper plate during subduction (e.g., Solari et al., 2007).

In southwestern Mexico, undeformed granitic bodies postdate the end of the Laramide shortening. In general, and at least for the studied area, previous works established the end of the Laramide deformation at ~55 Ma (e.g., Solari et al., 2007; Cerca et al., 2007).

Yet, geochemical and petrological data of those igneous bodies are scant and mainly focused on a few studied Oligocene rocks such as the Rio Verde Batholith (Hernández-Bernal and Morán-Zenteno, 1996) and the Tierra Colorada pluton (Schaaf, 1990; Herrmann et al., 1994), or on the Tertiary volcanic arc (e.g., Morán-Zenteno et al., 1999; Martiny et al., 2000).

Here, we present new geologic, geochemical isotopic, geochronologic, and thermobarometric data for the Acapulco intrusion that has been considered as an anomaly based on its age, composition, and petrologic characteristics that contrast with the surrounding plutons (mainly calc-alkaline granodiorites) and the general age trend from the coastal batholithic belt (between 35 and 30 Ma, Ducea et al., 2004a; Morán-Zenteno et al., 2007; Valencia et al., 2009). The aim of this paper is to elucidate the main petrogenetic processes involved in its evolution, as well as the tectonic implications of such an important

*Corresponding author, present address: Candiani Mining, Guillermo González Camarena 900B, piso1, Colonia Centro Ciudad Santa Fe, Álvaro Obregón, 01210 México, D.F., Mexico; gahp@exalumno.unam.mx.

Geosphere; December 2011; v. 7; no. 6; p. 1419–1438; doi:10.1130/GES00744.1; 11 figures; 4 tables.

intrusion that can provide valuable information for the post-Laramide magmatism and geological evolution in southern Mexico.

GEOLOGICAL FRAMEWORK

Southern Mexico is composed of a mosaic of contrasting crustal blocks that range in age from Grenvillian (Oaxacan Complex, e.g., Solari et al., 2003), to Paleozoic (Acatlán Complex, e.g., Ortega-Gutiérrez et al., 1999), and Mesozoic (Guerrero arc succession, Talavera-Mendoza et al., 2007; Centeno-García et al., 2008; Martini et al., 2009) (Fig. 1), which are the basis on which southern Mexico has been subdivided into several tectonostratigraphic terranes (e.g., Sedlock et al., 1993; Dickinson and Lawton, 2001; Keppie, 2004). The absence of forearc rocks toward the southern Pacific coast from Paleocene until Miocene times has been interpreted as the truncation of the continental margin of southern Mexico, and it was first observed and discussed by De Cserna (1965). Later studies focused on the tectonic reshaping of southwestern Mexico during the late Mesozoic and Tertiary, involving the displacement of the Chortís block from southern Mexico to its current position, combined with an important contribution of subduction erosion (e.g., Schaaf et al., 1995; Morán-Zenteno et al., 1996; Meschede et al., 1996; Ducea et al., 2004a; Keppie and Morán-Zenteno, 2005; Morán-Zenteno et al., 2005; Nieto-Samaniego et al., 2006; Solari et al., 2007; Keppie et al., 2009).

Active subduction along the southern margin of Mexico took place since the Early Jurassic (~180 Ma), but significant variations in subduction rates and in the age of the subducted lithosphere were produced since the Oligocene due to the fragmentation of the subducting Farallon plate into Nazca, Cocos, and Rivera (Engebretson et al., 1985).

The coastal batholithic belt intrudes the Xolapa Complex along its southeastern section. As first described by De Cserna (1965), the Xolapa Complex is a 600-km-long and 50–100-km-wide metamorphic belt that parallels the Pacific coast of southern Mexico (Fig. 1), composing the basement of the Xolapa terrane (Campa and Coney, 1983). The Xolapa Complex is made of a sequence of amphibolite-facies metamorphic rocks, repeatedly intruded by deformed and undeformed calc-alkaline plutonic rocks. Recent works by Solari et al. (2007) and Pérez-Gutiérrez et al. (2009) limited the definition of the Xolapa Complex to those rocks affected by migmatization and ductile deformation, which predate the ~130 Ma intrusion of unmetamorphosed granites (e.g., El Pozuelo granite).

The Acapulco intrusion has been considered as an enigmatic feature in the magmatic evolution of Mexico mainly because its age does not follow the regional trend from the coastal batholithic belt and because of its peculiar rapakivi texture. Nonetheless, modern analytical data

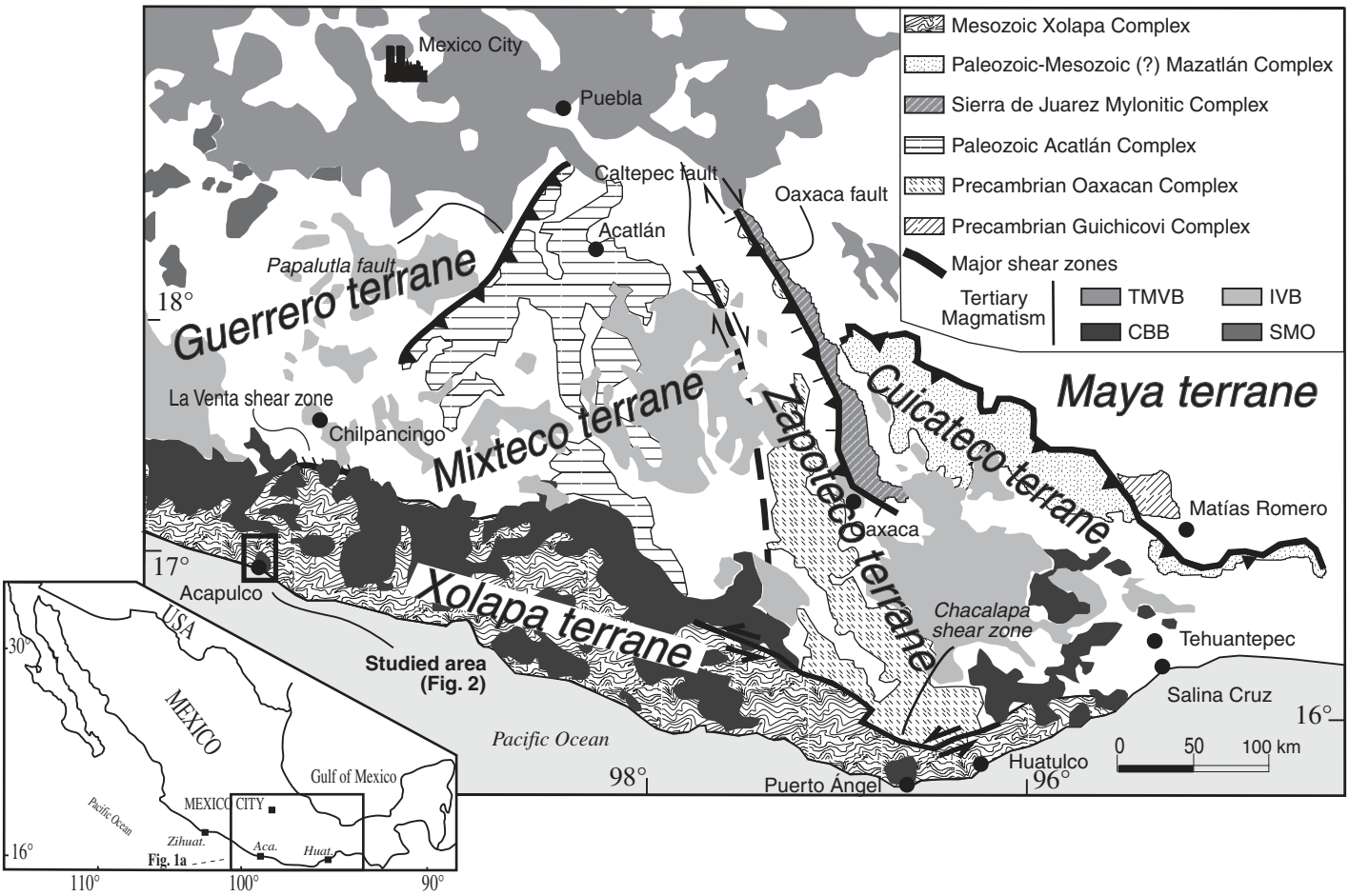

Figure 1. Simplified tectonostratigraphic division of southern Mexico with major Cenozoic magmatic belts (modified after Solari et al., 2007 and Morán-Zenteno et al., 2007). Abbreviations: TMVB—Trans-Mexican volcanic belt; IVB—Inland volcanic belt; CBB—coastal batholithic belt; SMO—Sierra Madre Occidental.

are not available, and its tectonic framework remains poorly understood. The Acapulco intrusion was first recognized by De Cserna (1965) as a composite stock with a composition ranging from monzogranite to quartz syenite. The first isotopic age reported on the granitic unit of this pluton was a Rb-Sr isochron calculated at 43.4 ± 0.9 Ma by Schaaf et al. (1995). Later on, Ducea et al. (2004a) dated the quartz-syenite unit of the Acapulco intrusion by LA-ICP-MS in zircons at 54.9 ± 2.0 Ma.

RECOGNIZED LITHOLOGIC UNITS

The lithologic units of the study area include (1) metamorphic basement, including those units that were originally sedimentary or igneous; (2) the Tamuchis deformed granite; and (3) the Acapulco intrusion.

Metamorphic Basement

Xolapa Complex

The exposed Xolapa Complex lithologies in the neighboring area of Acapulco (Fig. 2) correspond to those previously studied by Pérez-Gutiérrez et al. (2009). They are characterized by the occurrence of metasediments and orthogneisses with high-grade (amphibolitic) fabrics and a general WNW-trending, NNE-dipping metamorphic foliation (Fig. 3A).

Tamuchis Granite

The Tamuchis granite is a ductile deformed pluton that intrudes orthogneisses of the Xolapa Complex to the north of Acapulco city (Figs. 2 and 3B). NE-trending, SE-dipping metamorphic foliations are defined by amphibole and mica. Though no geochronological data are available, the Tamuchis granite is distinguished from the Acapulco intrusion by its deformed nature, and the lack of characteristic minerals that are present in the Acapulco granite (see below). The Tamuchis granite resembles the ~130 Ma deformed granites cropping out farther to the north, which slightly postdate the migmatization event (e.g., Solari et al., 2007).

Acapulco Intrusion

The Acapulco composite pluton was divided into three units based on their texture and composition.

Rapakivi Granite

This granitic unit is the largest and widespread on the studied area (Fig. 2). It consists of gray-colored granite with some pinkish zones and dark-gray schlieren textures, with 5-cm-thick bands along the entire unit. It contains pink orthoclase (Or), quartz (Qtz), and plagioclase (Pl) with hornblende (Hbl) and biotite (Bt) as accessory minerals. The principal characteristic of this granite is the development of rapakivi texture, i.e., potassic feldspar (Kfs) immersed in sodic plagioclase mantle (Fig. 3C) (Haapala and Ramö, 1990). Black to dark-gray mafic magmatic enclaves (MME) are abundant in this particular unit of the Acapulco intrusion. They are mostly made up of Bt, Hbl, and Pl with some Kfs crystals.

Whereas the albitic (Ab) plagioclase is only restricted to rapakivi mantles in this granite (*sensu stricto*) (Fig. 4A), oligoclase composition is found in plagioclase crystals present elsewhere in the groundmass (Fig. 4B). Every Kfs crystal within the rapakivi texture presents mesoperthitic textures as well (Fig. 4A). The most distinctive accessory phases under microscope are allanite (Aln) and fluorite (Fl) (Figs. 4C and 4D). Aln occurs as prismatic brown to pinkish crystals and are often zoned. Colorless and isotropic crystals of Fl are generally surrounded by Bt and Hbl (Fig. 4D). Other important accessory phases are titanite (Ttn), zircon (Zr), Ti-Fe oxides (e.g., magnetite [Mag] and ilmenite [Ilm]), and apatite (Ap). Ap shows two different shapes, some stubby to rounded, whereas other crystals are thin and elongated (Fig. 4C).

Under the microscope, the mafic enclaves are quartzodioritic to tonalitic in composition, with diffuse contacts with the granitic host rock and smaller crystal size (Fig. 4E). Big fine-grained clusters of Bt + Hbl + Ap + Tnt can be observed within a coarser Pl + Qz groundmass.

Quartz Syenite

The northwestern and eastern edges of the Acapulco intrusion are composed of quartz syenite (Fig. 2), but an intrusive contact with gneisses and schists of the Xolapa Complex can only be recognized at the southeastern edge (Fig. 2). Both quartz syenites are greenish to gray in color, with a phaneritic texture that allows macroscopic recognition of Kfs, amphibole, and Qz as the main mineral phases (Fig. 3D).

Under the microscope, they can be classified as quartz syenites. Microcline and Qz were identified as principal minerals, displaying mirmekitic textures. Albitic Pl is restricted to perthites within Kfs, where it can constitute up to 30% of the entire crystal. Most common accessory minerals are Hbl with relic orthopyroxene cores, minor biotite, allanite, Ti-Fe oxides, and zircon (Figs. 4F and 4G).

Diorites

Two previously unidentified dioritic units were recognized within the Acapulco intrusion (Fig. 2). They are dark gray to black in color, showing a phaneritic texture made up of amphibole and Pl crystals with minor pyroxene. We named El Derrumbe diorite a body that crops out along the road that connects Acapulco city with the town of Pie de la Cuesta (Fig. 2). This diorite is intruded by the rapakivi granite (Fig. 3E), which shows some dioritic xenoliths near the contact zone. On the other hand, we also named another body that crops out at the center of the studied area mingled with the rapakivi granite as the Carabalí diorite (Fig. 3F). Interestingly, some crystals with rapakivi texture can also be found within the diorite bodies.

Both mafic intrusives are mainly composed of Pl (labradoritic in composition) with minor Qz (Figs. 4H and 4I). Their characteristic dark color is given by the high amount of mafic minerals, dominated by Hbl and Bt, with the former more abundant than the latter (Fig. 4I).

ANALYTICAL PROCEDURES

A total of 17 samples were collected for geochemical analyses. Major elements were determined by X-ray fluorescence (XRF) spectroscopy using a Siemens SRS-3000 instrument installed at the Laboratorio Universitario de Geoquímica Isotópica (LUGIS, Universidad Nacional Autónoma de México [UNAM]), following the procedures described by Lozano-Santa Cruz et al. (1995). Trace-element data were obtained by inductively coupled plasma–mass spectrometry (ICP-MS) at Laboratorio de Estudios Isotópicos (LEI), at Centro de Geociencias (CGEO, UNAM), using a Thermo X Series II instrument. Because most of the studied intrusive rocks contain zircon, the digestion procedure described by Mori et al. (2007) for low-pressure vessels was modified to ensure complete solution. Rock powders were first digested in a mixture of HF + HNO_3 and then diluted to 3 mL in 4N HNO_3 and further centrifuged. Solid residuals were separated and re-digested in 500 µl of HF and 250 µl of 8N HNO_3 and put into a high-pressure Parr vessel at 200 °C for a period of four days. Digested residuals were dried and refluxed overnight with concentrated HNO_3 to break down insoluble fluorides. The two sample splits were then mixed together, evaporated to dryness, and later diluted to 1:2000 to provide adequate concentrations within the instrument detection limits and to yield the correct signals required for high-precision data. Data acquisition procedures and typical reproducibility follow those described by Mori et al. (2007).

Isotopic determinations were performed at LUGIS (UNAM) for both WR and feldspar separates. Sr, Sm, Nd, and Pb isotopic ratios were obtained using isotope dilution–thermal ionization mass spectrometry (ID-TIMS) following

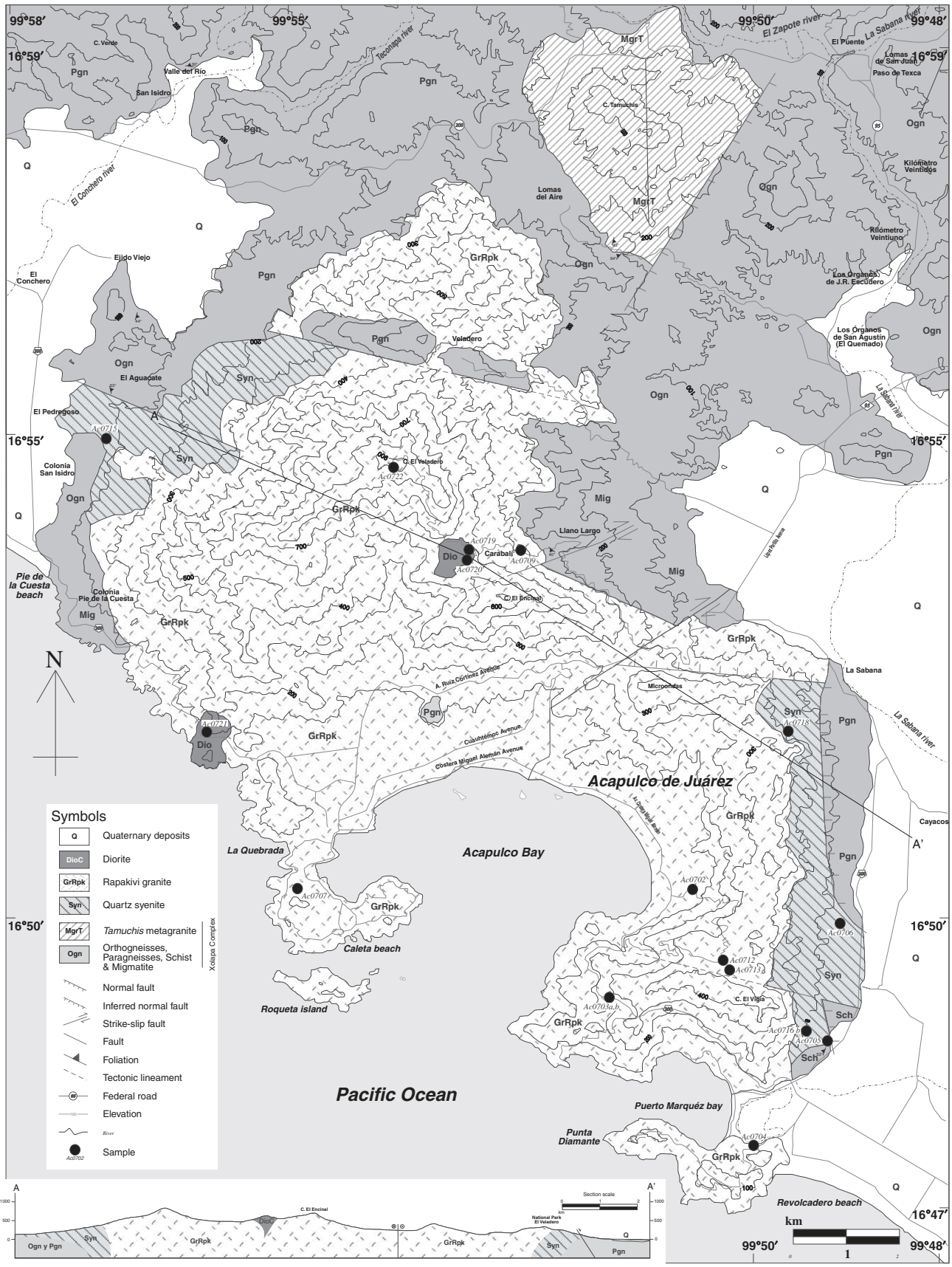

Figure 2. Geologic map and cross section of the Acapulco area.

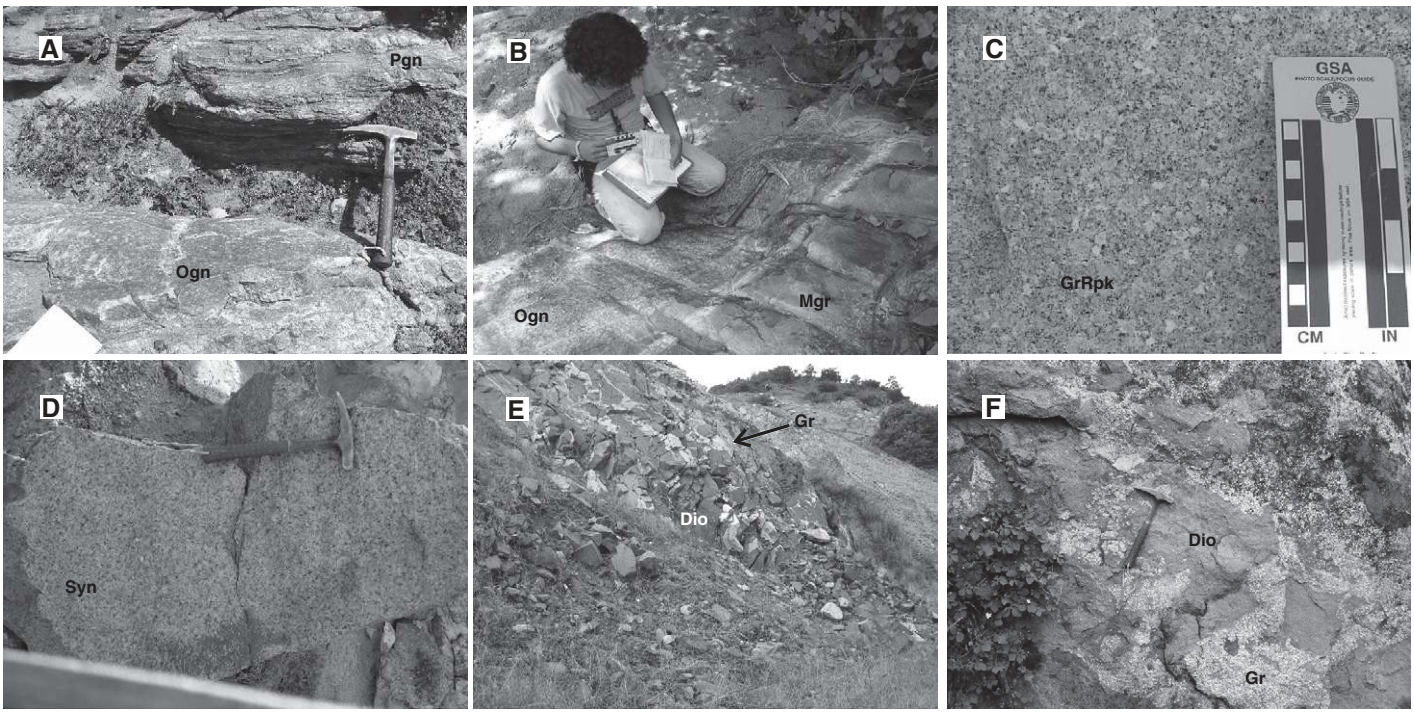

Figure 3. Pictures showing the general aspect of selected outcrops from the different Acapulco intrusion area lithologies: (A) Intrusive contact between orthogneisses and paragneisses along the Teconapa River; (B) main contact between the Tamuchis granite and orthogneisses from the Xolapa Complex; (C) general aspect of the rapakivi texture from the Acapulco granite near Puerto Marquez bay area; (D) quartz-syenite block next to the contact with Xolapa Complex gneisses on the eastern boundary of the Acapulco intrusion; (E) rapakivi granite intrusion into El Derrumbe diorite; (F) mingled contacts between the Carabalí diorite and the rapakivi granite near Carabalí town. Abbreviations: Pgn—paragneisses; Ogn—orthogneisses; Mgr—Tamuchis metagranite; GrRpk—rapakivi granite; Syn—quartz syenite; Dio—diorite.

the standard methods described by Schaaf et al. (2005) and Solari et al. (2004), using a Finnigan MAT262 mass spectrometer equipped with eight Faraday detectors. Rb isotopic ratios were measured with a National Bureau of Standards (NBS)-type single collector mass spectrometer as described by Schaaf et al. (2000). Zircons separated from four samples were dated by LA-ICP-MS U-Pb geochronology at LEI, using the instrumentation and procedures described in Solari et al. (2010). Unknown ages were calculated employing the 91500 standard zircon (Wiedenbeck et al., 1995) as bracketing standard. The Tuff-Zirc algorithm (Ludwig and Mundil, 2002) was used to calculate the mean $^{206}Pb/^{238}U$ ages and their errors, as well as to filter for outliers. Such age calculation is preferred for Phanerozoic ages obtained by LA-ICP-MS, due to the uncertainty of ^{207}Pb determination.

Electron-microprobe analyses were performed at Stanford University using a JEOL JXA-733A superprobe fitted with five wavelength-dispersive spectrometers and a Be-window SiLi energy-dispersive detector, and 15 kv, 20 nA, and 20 s as instrument settings. Standards and crystals used were: Na (albite), Mg (olivine), Al (spessartine), Si (wollastonite), K (orthoclase), Ca (wollastonite), and Fe (hematite). Plagioclase analyses were performed with a defocused electron beam at 10 μm due to the complexity of Na measurements. Each crystal was analyzed three times for statistical control. Quantitative analyses were performed using the CITZAF matrix correction algorithm (Armstrong, 1988). Relative standard deviations for major oxide components were 1%, 10% for minor elements, and 15% for trace elements.

RESULTS

Major- and Trace-Element Geochemistry

Major- and trace-element abundances are reported in Table 1. In general, the Acapulco intrusion rocks vary between 51.49 and 76.95 wt% SiO_2, whereas Al_2O_3 is in the range 12.25 to 17.06 wt%, K_2O from 1.40 to 5.10 wt%, Na_2O from 3.36 to 5.31 wt%, CaO from 0.28 to 7.43 wt%, MgO from 0.10 to 6.23 wt%, TiO_2 from 0.07 to 1.26 wt%, FeO* from 1.32 to 10.19 wt%, and P_2O_5 from 0.01 to 0.28 wt%. Major elements show negative correlation with SiO_2 except for K_2O and Na_2O (Fig. 5). This behavior may represent crystal fractionation of plagioclase, apatite, ilmenite, and titanite during the crystallization of the Acapulco intrusion.

The Acapulco samples can be classified as diorite, granite, and syenite in a total alkali versus silica (TAS) diagram for plutonic rocks according to Wilson (1989) (Fig. 5A), and belong to the calc-alkaline series in an AFM diagram (Irvine and Baragar, 1971). Using the Shand's index of alumina saturation, the Acapulco intrusion classifies as metaluminous (e.g., diorites) to slightly peraluminous granite (Maniar and Piccoli, 1989) (Fig. 5B).

Eu and Sr contents correlate negatively with SiO_2, whereas Nb, Ta, U, and Th have positive correlations due to the highly incompatible behavior of the lithophile elements (Fig. 5). Rocks from the Acapulco intrusion have high large-ion lithophile to high field strength element (LIL/HFSE) ratios that are common in subduction related magmas, but often display strong Ba, Sr, and Eu negative anomalies in primitive-mantle–normalized trace-element diagrams (Fig. 6A). They also show enriched light rare-earth element (LREE), flat heavy rare-earth

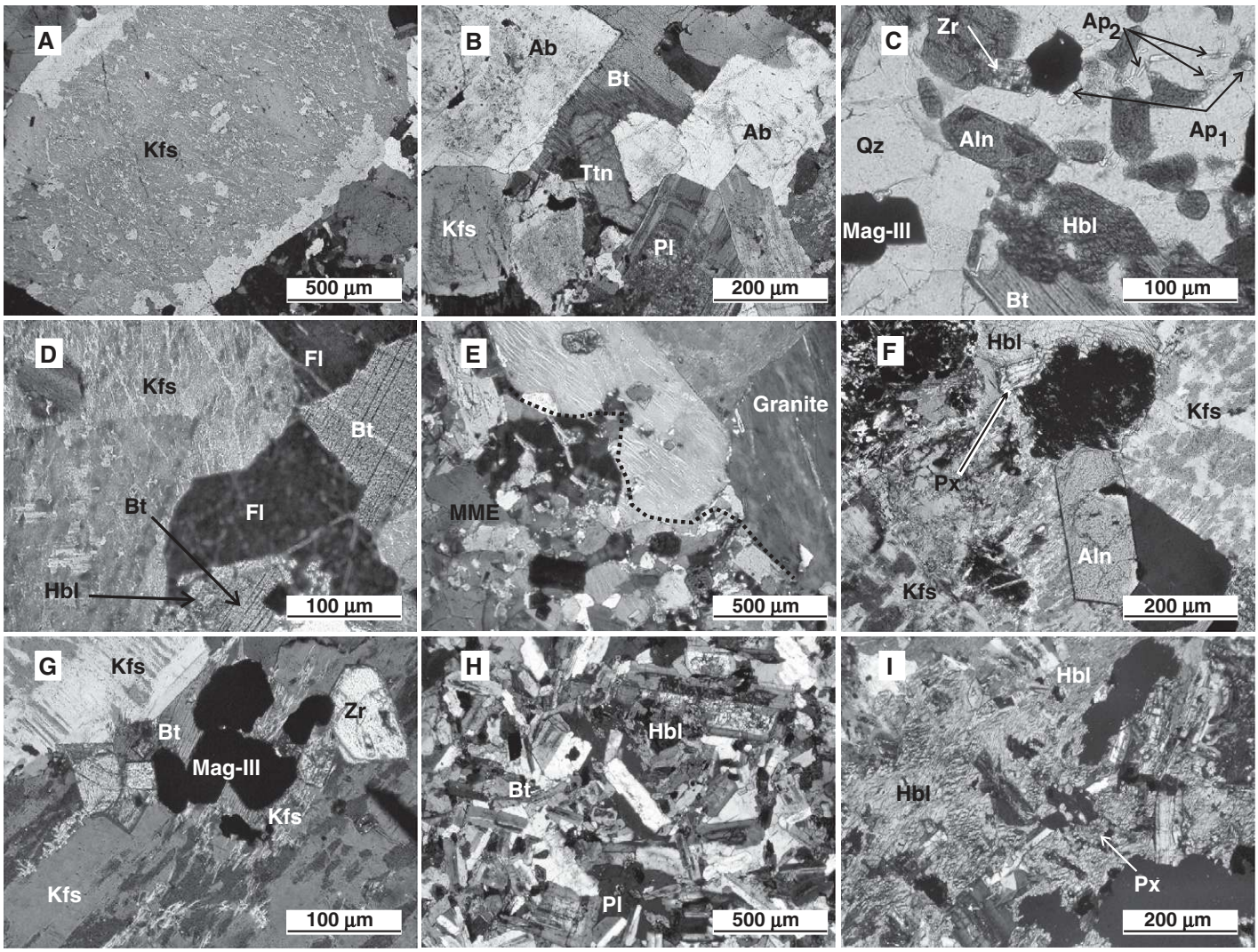

Figure 4. Photomicrographs showing petrographic and textural aspects of the Acapulco intrusion lithologies: (A) General aspect of the rapakivi texture: perthitic K-feldspar rimmed by plagioclase mantles; (B) crossed polarized view of an accessory minerals cluster (biotite and titanite) in contact with albite, K-feldspar and non-rapakivi related plagioclase; (C) minor accessory phases (allanite, apatite, zircon, and magnetite-ilmenite) immerse in a quartz + biotite + hornblende mass; (D) occurrence of subhedral fluorite crystals in contact with biotite crystals, one of them is rimmed by hornblende; (E) mineral and textural contrast along the contact between the rapakivi granite and a mafic magmatic enclave; (F) general aspect of the quartz-syenite, showing hornblende crystals with pyroxene relics, allanite and the characteristic perthitic texture; (G) accessory minerals contained in the quartz-syenite: biotite, Fe-Ti oxides and zircon; (H) general textural aspect of the Carabalí diorite with hornblende and biotite as the major accessory minerals; and (I) hornblende phenocrysts with relic pyroxene from El Derrumbe diorite.

element (HREE) patterns in CI-chondrite normalized diagrams (Fig. 6B). Such high LREE values (La = 12.72–82.15 ppm) and low Yb (2.33–11.73 ppm) represent La/Yb rations between 1.4 and 25.1.

Even though the Acapulco rocks show arc-related trace-element patterns, they plot at the limit between volcanic arc granites (VAG) to within-plate granites (WPG) in a Y + Nb versus Rb diagram (Pearce et al., 1984) (Fig. 7A). A similar behavior can be found in the classic I&S type and A-type granite discrimination diagram (Whalen et al., 1987) (Fig. 7B). Nonetheless, the most mafic diorite samples invariably plot within the field of arc-related magmas in both diagrams (Figs. 7A and 7B).

Sr-Nd-Pb Isotopes

Results for Sr-Nd-Pb isotopic determinations are shown in Table 2. Initial isotopic ratios for the Acapulco intrusion samples are highly variable for $^{87}Sr/^{86}Sr$ from 0.7035 up to 0.7100, while $^{143}Nd/^{144}Nd$ ratios are almost constant, ranging from 0.51266 to 0.51272, except for El Derrumbe diorite, which has a ratio of 0.51285. Samples plot along the coastal batholithic belt field of Morán-Zenteno et al. (1999) (Fig. 7C). Even with such variations, most Acapulco samples fit within the normal mantle array represented by mid-ocean ridge basalts (MORBs) and ocean island basalts (OIBs), with the Sierra Nevada of California rocks representing a continental magmatic arc suite (Fig. 7C). On the other hand, Pb isotopes show an almost homogenous behavior with slightly higher $^{206}Pb/^{204}Pb$ and $^{207}Pb/^{204}Pb$ values compared to Pacific-type

TABLE 1. MAJOR AND TRACE ELEMENT

Sample	Ac 0702	Ac 0703a	Ac 0703b	Ac 0704	Ac 0705	Ac 0706	Ac 0707	Ac 0709	Ac 0712	Ac 0713	Ac 0715	Ac 0716b	Ac 0718	Ac 0719	Ac 0720	Ac 0721	Ac 0722
Lithology	Granite	Granite	MME	Granite	QzSyenite	QzSyenite	Granite	Granite	Granite	Granite	QzSyenite	QzSyenite	QzSyenite	Diorite	Diorite	Diorite	Granite
Longitude W	99°50′24″	99°51′28″	99°51′28″	99°49′53″	99°49′09″	99°48′58″	99°54′50″	99°52′27″	99°50′00″	99°49′59″	99°56′59″	99°49′20″	99°49′29″	99°53′02″	99°52′58″	99°56′04″	99°53′50″
Latitude N	16°50′05″	16°49′06″	16°49′06″	16°47′36″	16°48′31″	16°49′57″	16°50′16″	16°53′41″	16°49′27″	16°49′23″	16°54′59″	16°48′51″	16°51′49″	16°53′43″	16°53′39″	16°52′05″	16°54′42″
SiO_2	73.1	72.3	60.0	73.8	74.6	74.0	71.2	73.4	74.4	71.1	76.8	65.5	76.5	60.6	61.3	50.5	74.1
TiO_2	0.27	0.30	1.10	0.25	0.13	0.16	0.28	0.34	0.19	0.32	0.07	0.44	0.09	0.90	0.91	1.24	0.21
Al_2O_3	13.6	14.1	16.3	12.6	12.9	13.0	14.2	13.3	13.4	14.1	12.2	16.8	12.2	16.0	15.8	16.7	13.1
$Fe_2O_{3\ t}$	2.37	2.45	7.82	2.42	1.96	2.43	2.81	2.78	1.68	2.95	1.46	3.99	1.58	7.24	7.16	11.1	2.16
MnO	0.04	0.05	0.20	0.05	0.05	0.05	0.07	0.05	0.02	0.06	0.04	0.09	0.04	0.11	0.14	0.16	0.04
MgO	0.26	0.36	1.57	0.84	0.12	0.10	0.47	0.57	0.41	0.61	0.11	0.51	0.11	2.64	2.31	6.12	0.34
CaO	1.13	1.36	4.09	0.99	0.47	0.44	1.01	1.49	1.13	1.50	0.28	1.81	0.36	5.17	4.59	7.29	0.73
Na_2O	3.90	3.85	5.03	3.68	4.34	4.50	4.26	3.80	3.97	4.18	4.13	5.28	4.09	3.70	4.26	3.30	4.08
K_2O	4.57	4.68	1.85	4.57	5.02	4.94	5.07	4.18	4.42	4.56	4.63	4.91	4.66	2.77	2.58	1.37	4.56
P_2O_5	0.07	0.09	0.48	0.07	0.02	0.02	0.09	0.09	0.08	0.10	0.01	0.09	0.01	0.23	0.22	0.27	0.07
LOI	0.34	0.43	1.32	0.55	0.26	0.32	0.39	0.31	0.31	0.40	0.25	0.34	0.32	0.44	0.48	1.71	0.53
Total	99.7	100.0	99.8	99.8	100.0	100.0	99.8	100.4	100.1	100.0	100.1	99.8	100.0	99.8	99.8	99.8	100.0
V	18.5	20.6	106	17.3	4.66	5.00	16.0	19.00	13.0	23.3	4.55	13.0	5.00	146	160	216	11.2
Cr	128	108	64.3	122	132	125	113	118	146	93.3	144	79.2	170	75.2	77.0	46.8	103
Co	3.53	3.56	9.07	3.53	1.91	6.00	3.21	6.00	6.00	3.92	2.00	2.89	6.00	16.1	11.0	41.0	2.59
Ni	4.36	4.09	4.09	4.36	3.80	7.00	4.08	8.00	8.00	3.84	4.13	3.25	9.00	7.11	9.00	67.3	3.72
Cu	2.76	2.58	5.75	4.73	1.71	3.00	2.68	2.00	3.00	2.73	1.59	4.13	4.00	11.4	6.00	78.1	2.00
Zn	47.8	44.8	138	65.0	44.4	140	70.5	63.0	42.0	52.3	31.6	73.8	59.0	81.3	111	95.0	50.4
Ga	19.3	18.8	29.1	17.8	19.7	N.D.	22.4	N.D.	N.D.	19.6	19.5	20.7	N.D.	18.8	N.D.	18.3	20.6
Rb	168	163	143	163	87.3	193	171	163	153	155	123	89.2	169	101	116	43.9	177
Sr	81.5	103	158	71.7	7.31	3.00	75.2	121	102	104	4.41	170	2.00	299	302	432	57.7
Y	43.9	38.8	132	33.5	32.1	57.0	76.3	47.0	30.0	43.1	40.0	35.4	63.0	31.4	32.0	25.1	45.4
Zr	211	181	183	128	203	503	207	191	134	106	136	571	231	174	173	122	216
Nb	15.7	14.4	49.8	13.5	11.6	21.0	30.9	14.0	10.0	16.3	10.8	17.2	24.0	8.00	7.00	5.11	18.1
Mo	2.55	2.18	1.78	2.54	3.44	N.D.	3.28	N.D.	N.D.	2.24	2.79	2.76	N.D.	2.46	N.D.	2.58	2.75
Sn	4.27	2.96	11.5	4.72	1.79	N.D.	4.58	N.D.	N.D.	3.76	1.50	2.36	N.D.	2.80	N.D.	2.59	5.33
Sb	0.22	0.22	0.48	0.24	0.22	N.D.	0.26	N.D.	N.D.	0.09	0.19	0.16	N.D.	0.12	N.D.	0.24	0.23
Cs	4.77	4.32	7.77	3.17	1.74	N.D.	4.65	N.D.	N.D.	3.64	1.82	3.43	N.D.	3.19	N.D.	2.01	5.12
Ba	346	506	238	310	31.0	22.0	372	428	424	445	14.6	3049	19.0	578	518	357	278
La	39.5	51.9	16.5	34.6	82.1	N.D.	48.8	N.D.	N.D.	35.0	38.9	24.6	N.D.	22.0	N.D.	12.7	52.0
Ce	79.0	102	51.4	70.3	149	N.D.	105	N.D.	N.D.	71.8	74.6	51.3	N.D.	44.5	N.D.	28.3	105
Pr	9.54	12.1	9.01	8.45	17.0	N.D.	13.8	N.D.	N.D.	8.99	8.89	6.89	N.D.	5.66	N.D.	3.95	12.6
Nd	35.2	43.1	44.7	30.8	59.3	N.D.	54.1	N.D.	N.D.	34.3	32.2	28.8	N.D.	22.7	N.D.	17.5	45.3
Sm	7.32	8.13	14.7	6.16	9.33	N.D.	12.4	N.D.	N.D.	7.62	6.60	6.66	N.D.	5.22	N.D.	4.32	8.81
Eu	0.50	0.60	0.90	0.44	0.13	N.D.	0.53	N.D.	N.D.	0.59	0.09	2.25	N.D.	1.24	N.D.	1.28	0.41
Tb	1.13	1.08	2.90	0.89	1.04	N.D.	2.06	N.D.	N.D.	1.17	1.06	1.03	N.D.	0.84	N.D.	0.70	1.26
Gd	6.74	6.77	16.4	5.54	7.03	N.D.	12.0	N.D.	N.D.	7.15	6.33	6.34	N.D.	5.19	N.D.	4.39	7.71
Dy	6.99	6.34	18.9	5.41	5.68	N.D.	12.8	N.D.	N.D.	7.19	6.63	6.23	N.D.	5.23	N.D.	4.28	7.56
Ho	1.44	1.28	3.90	1.10	1.13	N.D.	2.58	N.D.	N.D.	1.44	1.35	1.26	N.D.	1.07	N.D.	0.88	1.53
Er	4.26	3.76	11.4	3.21	3.30	N.D.	7.31	N.D.	N.D.	4.18	3.87	3.58	N.D.	3.07	N.D.	2.46	4.45
Yb	4.52	3.86	11.5	3.18	3.27	N.D.	6.43	N.D.	N.D.	4.07	3.62	3.57	N.D.	3.07	N.D.	2.33	4.40
Lu	0.69	0.59	1.73	0.49	0.53	N.D.	0.93	N.D.	N.D.	0.61	0.54	0.58	N.D.	0.47	N.D.	0.36	0.66
Hf	6.05	5.20	6.07	3.98	5.20	N.D.	6.02	N.D.	N.D.	3.33	4.17	11.3	N.D.	4.48	N.D.	2.96	5.99
Ta	1.36	1.32	3.91	0.92	0.71	N.D.	1.58	N.D.	N.D.	1.18	0.85	1.04	N.D.	0.68	N.D.	0.33	1.28
W	0.56	0.55	0.54	0.56	0.56	N.D.	0.55	N.D.	N.D.	0.54	0.56	0.54	N.D.	0.53	N.D.	0.52	0.55
Tl	1.03	1.01	0.98	1.10	0.52	N.D.	1.05	N.D.	N.D.	0.92	0.66	0.59	N.D.	0.67	N.D.	0.45	1.25
Pb	18.2	22.2	12.1	19.1	8.93	9.00	14.3	13.0	13.0	12.6	10.4	13.3	14.0	9.02	7.00	4.80	17.1
Th	13.9	16.1	14.6	42.6	8.88	17.0	10.9	16.0	9.00	10.6	9.66	4.66	16.0	5.90	7.00	1.26	15.2
U	3.66	4.10	9.07	12.9	2.28	N.D.	2.71	N.D.	N.D.	2.42	3.47	2.24	N.D.	2.24	N.D.	0.55	4.43

Note: Major elements (in wt %) were analyzed by XRF. Trace elements (in ppm) were analyzed by ICP-MS. MME—Mafic Magmatic Enclave; N.D.—not determined.

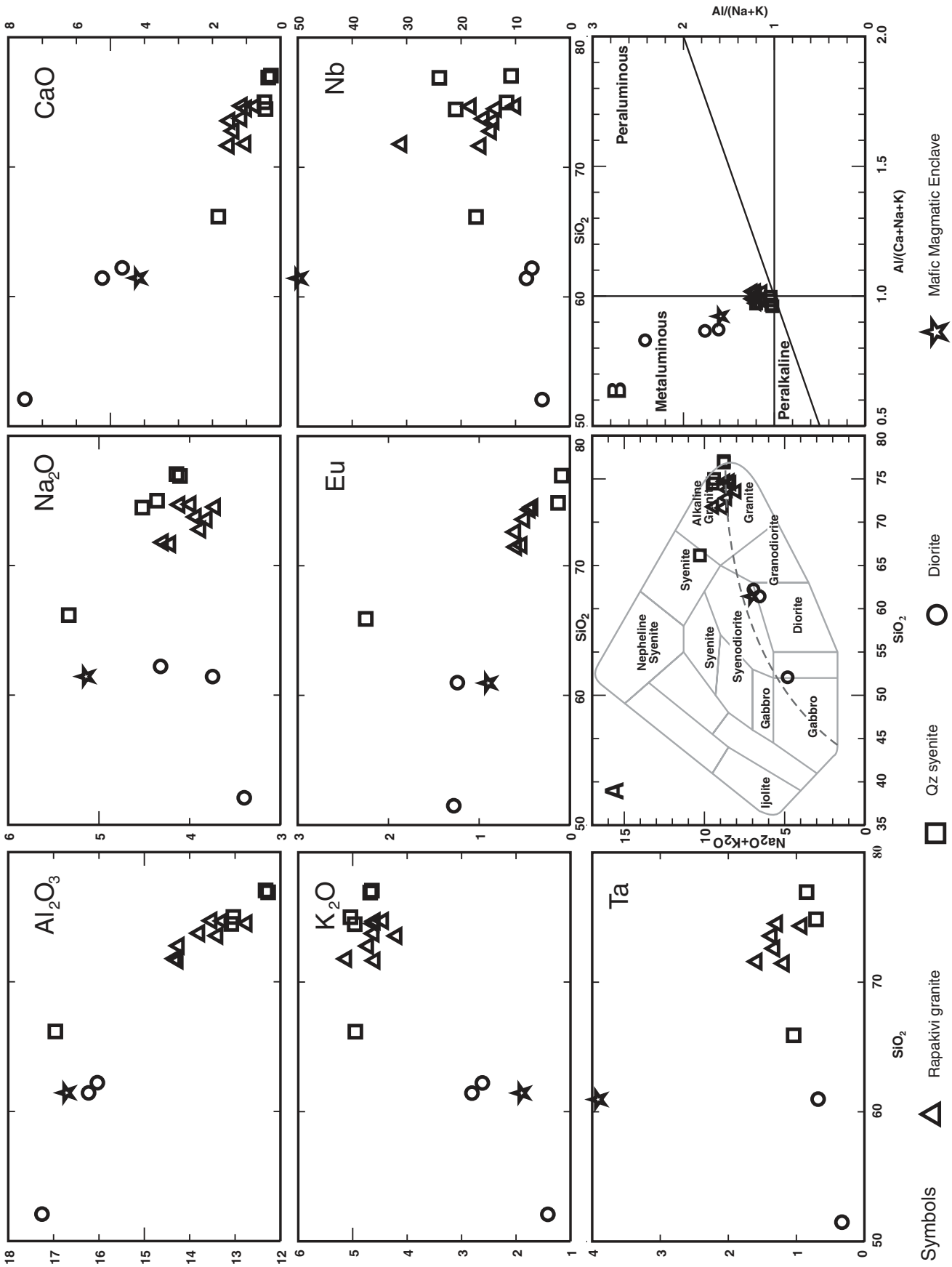

Figure 5. Silica variation diagrams of selected major and trace elements for rocks of the Acapulco intrusion. All data are normalized to 100 wt% on anhydrous basis. (A) Total alkali versus silica (TAS) classification diagram for plutonic rocks (after Wilson, 1989). (B) Shand's alumina saturation index (Maniar and Piccoli, 1989).

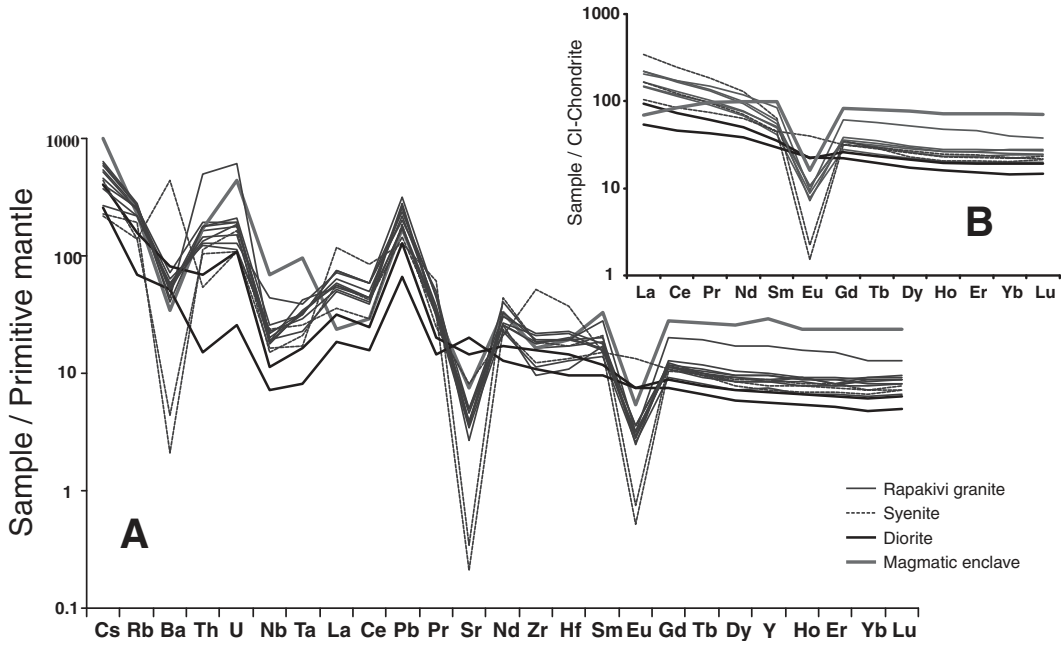

Figure 6. Trace multielemental diagrams: (A) Spider diagram of trace elements normalized to the primitive mantle composition according to Sun and McDonough (1989); (B) rare-earth element patterns normalized to the CI chondrite of McDonough and Sun (1995).

MORB ratios (Ito et al., 1987), although they are lower than those from the Xolapa Complex (mid-crust basement, Herrmann et al., 1994; Pérez-Gutiérrez et al., 2009), displaying a positive trend almost parallel to the Grenvillian Oaxacan Complex (lower-crust basement, Solari et al., 2004) (Fig. 7D).

U-Pb Geochronology

Zircons separated from three samples of the rapakivi granite and one more from the quartz syenite are generally euhedral, prismatic, and colorless to amber. They show D, P_5, and P_4 morphologies according to Pupin (1980, 1988), with a maximum elongation ratio of 3:1 and general size of ~200 μm. Cathodoluminescence (CL) images of these samples show oscillatory zoning indicative of a magmatic origin, which sometimes grows around inherited, igneous cores. Results of U-Pb dating by LA-ICP-MS are shown in Table 3. Using the Tera-Wasserburg diagrams plotted with Isoplot/Ex v. 3.60 (Ludwig, 2008), the samples from the rapakivi granite (Ac0702, Ac0707, and Ac0722) yield ages of 50.20 ± 1.0 Ma (Fig. 8A), 50.56 ± 0.39 Ma, and 50.42 ± 0.39 Ma, respectively (Figs. 8C and 8D). Zircons from the quartz syenite yield a $^{206}Pb/^{238}U$ mean age of 49.40 ± 0.40 Ma (Fig. 8B). All ages are interpreted as crystallization ages and constrain the emplacement of the Acapulco intrusion at ~50 Ma. Those cores, which were also dated, are only slightly older than the obtained mean ages of 2–3 Ma. This indicates that such ages reflect the initial stage of zircon crystallization in the magma chamber, and that the Acapulco intrusion is practically devoid of xenocrystic, inherited nuclei belonging to the host rock. The age of ca. 50 Ma that we calculated for the Acapulco intrusion is slightly younger than the previous, 54.9 ± 2 Ma age obtained by Ducea et al. (2004a). We think that such difference reflects the variation of zircon crystallization and residence in the magma chamber, the same as in the case of the sample dated by Ducea et al. (2004a) has a spreading of 12 Ma (their Fig. 6a).

Thermometry and Barometry

Electron microprobe analyses were performed in different samples from the Acapulco granite, and the results are shown in Table 4. We analyzed coupled crystals (Pl and Hbl) in order to determine thermobarometric conditions following the methodology proposed by Anderson (1996), which requires emplacement temperatures to solve the corresponding geobarometric equations. In this study, we used Holland and Blundy (1994) Hbl-Pl thermometer "B" for the Edenite-Richterite system. Temperatures in Celsius degrees were calculated using HbPl v.1.2 software, yielding values between 692 and 737 °C with no apparent reequilibration (Table 4). Furthermore, the Ti content in zircons from the LA-ICP-MS analyses was used (Table 3), in order to apply the Ti-in-zircon thermometric determinations following the equations of Ferry and Watson (2007) yielding average temperatures of 739 °C (Table 3), which confirms the range of temperatures calculated with the Hbl-Pl geothermometer.

According to the mineral association observed in the rapakivi granite: two feldspars + quartz + biotite + hornblende + Fe-Ti oxides + titanite + apatite, we used the Al-in-hornblende barometer from Anderson and Smith (1995), modified from Schmidt (1992), with temperature as a parameter and the incorporation of experimental data of Johnson and Rutherford (1989). We applied these analysis to mineral clusters that show equilibrium textures, in particular with plagioclase that are not rapakivi texture related, and the main objective was to constrain a more accurate determination. All analyses together yield emplacement pressures between 2.08 and 2.84 kbar corresponding to 7.84–10.73 km depth (Table 4).

DISCUSSION

The new data presented in this study allow a better understanding of the emplacement and cooling conditions of the Acapulco intrusion, as well as the role of such plutons in the post-Laramide tectono-magmatic activity of southern Mexico. In this section we discuss the petrogenesis and evolution of the Acapulco intrusion and its implications, going from the microscopic scale to the regional tectonic context.

Significance of Accessory Minerals

The presence of fluorite in the Acapulco intrusion indicates the magmatic fluids evolved under fluorine saturation conditions. According to the observed crystallization order, hydrous minerals (particularly Bt and Hbl) preceded Fl

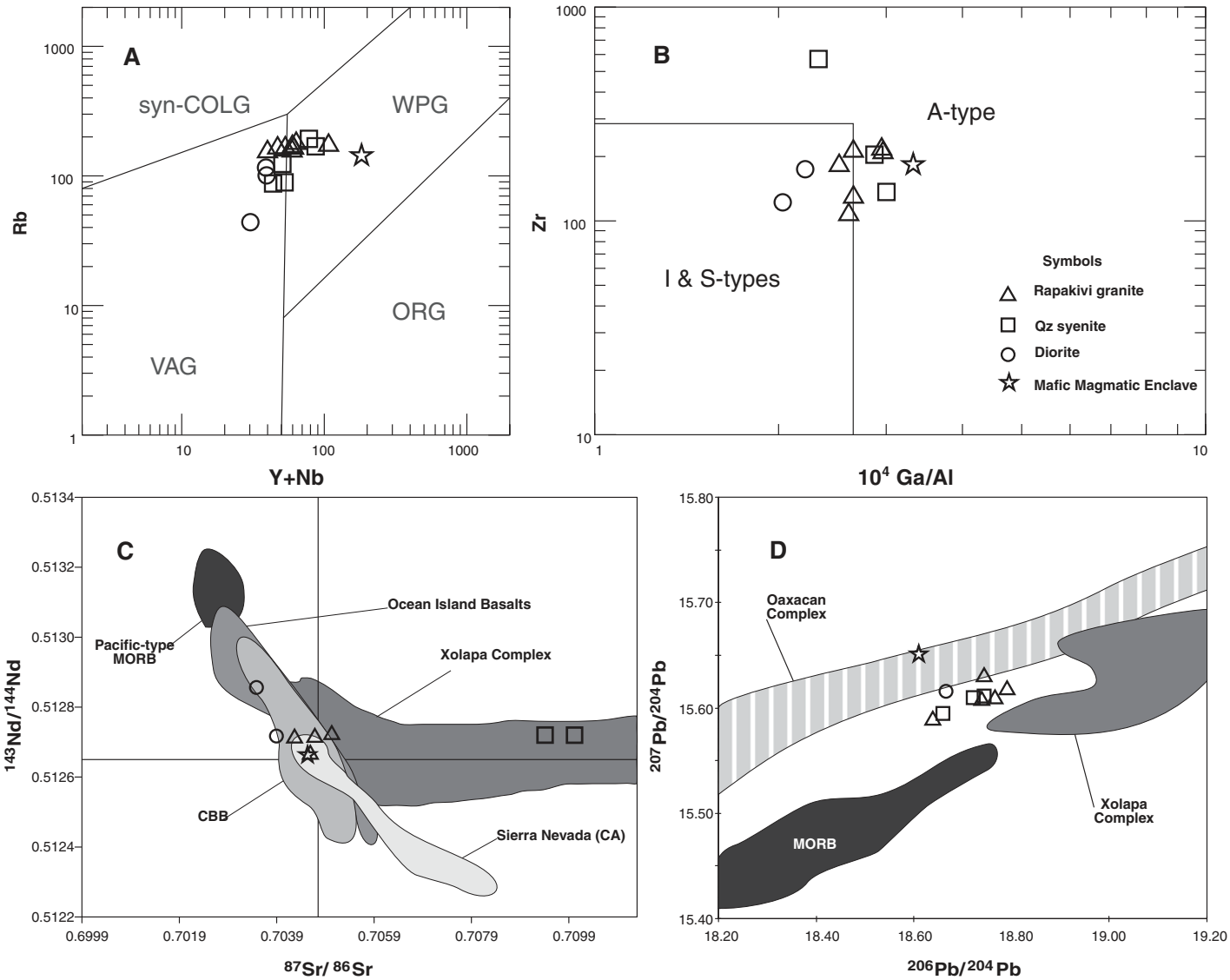

Figure 7. (A) Tectonic discrimination diagram Y + Nb versus Rb after Pearce et al. (1984): syn-COLG—syncollisional granites; VAG—volcanic-arc granites; WPG—within-plate granites; ORG—ocean-ridge granites. (B) Granitic typology discrimination diagram after Whalen et al. (1987). (C) $^{87}Sr/^{86}Sr$ versus $^{143}Nd/^{144}Nd$ initial ratios from the Acapulco intrusion calculated assuming a U-Pb age of 50 Ma. (D) $^{206}Pb/^{204}Pb$ versus $^{207}Pb/^{204}Pb$ isotopic ratios form the Acapulco intrusion compare with different isotopic signatures (WR Pb isotopes are age-corrected at 50 Ma). Mid-ocean ridge basalt (MORB) data from Ito et al. (1987); ocean island basalts from GEOROC (Nohl and Sarbas, 1999); Sierra Nevada values from North American volcanic and intrusive rocks (NAVDAT): Walker et al. (2006). Coastal batholithic belt (CBB) values are from Morán-Zenteno (1992); Herrmann et al. (1994); Schaaf et al. (1995); Hernández-Bernal and Morán-Zenteno (1996). Oaxacan Complex data are from Solari et al. (2004). Xolapa Complex data are from Morán-Zenteno (1992); Herrmann et al. (1994); Pérez-Gutiérrez et al. (2009).

TABLE 2. Sr, Nd AND Pb ISOTOPE COMPOSITIONS

Sample	Analysis Sr-Nd	Analysis Pb	$^{87}Sr/^{86}Sr \pm 1\sigma$	$^{143}Nd/^{144}Nd \pm 1\sigma$	$^{206}Pb/^{204}Pb$	1σ (%)	$^{207}Pb/^{204}Pb$	1σ (%)	$^{208}Pb/^{204}Pb$	1σ (%)
AC0702	WR	Kfs	0.708402 ± 38	0.512709 ± 21	18.7675	0.038	15.6099	0.038	38.5625	0.039
AC0703b	WR	WR	0.706124 ± 41	0.512727 ± 18	18.9760	0.097	15.6686	0.104	38.7786	0.124
AC0705	WR	Kfs	0.737901 ± 39	0.512749 ± 17	18.7223	0.039	15.6091	0.038	38.5444	0.039
AC0707	WR	Kfs	0.708934 ± 37	0.512763 ± 17	18.7453	0.035	15.6310	0.038	38.6147	0.046
AC0713	WR	Kfs	0.707185 ± 39	0.512747 ± 15	18.7395	0.037	15.6087	0.042	38.5437	0.048
AC0715	WR	WR	0.805392 ± 37	0.512758 ± 17	18.8237	0.080	15.6017	0.094	38.6200	0.108
AC0719	WR	WR	0.704530 ± 38	0.512761 ± 20	18.7885	0.102	15.6208	0.100	38.6409	0.100
AC0721	WR	WR	0.703665 ± 35	0.512902 ± 17	18.6957	0.181	15.5923	0.196	38.4824	0.194
AC0722	WR	Kfs	0.710698 ± 36	0.512764 ± 19	18.7242	0.044	15.6084	0.050	38.5397	0.058

Note: Reported values are not age corrected. WR—whole rock; Kfs—potassic feldspar. 1σ error for individual Sr and Nd measurements are multiplied by 10^6.

TABLE 3. U-Pb

				CORRECTED RATIOS†									CORRECTED AGES (Ma)									
	U (ppm)*	Th (ppm)*	Th/U	$^{207}Pb/^{206}Pb$	±1σ§	$^{207}Pb/^{235}U$	±1σ§	$^{206}Pb/^{238}U$	±1σ§	$^{208}Pb/^{232}Th$	±1σ§	Rho	$^{206}Pb/^{238}U$	±1σ	$^{207}Pb/^{235}U$	±1σ	$^{207}Pb/^{206}Pb$	±1σ	Best age (Ma)	±1σ	Ti-in T°C#	±1σ
Ac0702																						
AC0702_51_080	430	134	0.28	0.04855	1.480E-03	0.05467	0.00206	0.00817	0.00011	0.00259	0.00003	0.48	52.4	0.7	54	2	126	71	52.4	0.7	716	3.1
AC0702_47_074	432	413	0.87	0.04609	1.320E-03	0.04747	0.00181	0.00747	0.00011	0.00243	0.00006	0.4	48	0.7	47	2	2	50	48	0.7	915	0.1
AC0702_45_070	239	80	0.30	0.05258	2.560E-03	0.05811	0.00306	0.00802	0.00008	0.00251	0.00003	0.26	51.5	0.5	57	3	311	98	51.5	0.5	bdl	bdl
AC0702_39_062	614	251	0.37	0.0463	1.460E-03	0.05018	0.00189	0.00786	0.0001	0.00251	0.00007	0.47	50.5	0.7	50	2	13	61	50.5	0.7	717	3
AC0702_35_056	186	95	0.46	0.04876	1.990E-03	0.05274	0.00241	0.00784	0.00009	0.00248	0.00003	0.28	50.4	0.6	52	2	136	90	50.4	0.6	753	2.6
AC0702_34_055	386	134	0.32	0.04816	1.710E-03	0.05173	0.00207	0.00779	0.00009	0.00247	0.00004	0.34	50	0.6	51	2	107	78	50	0.6	bdl	bdl
AC0702_32_053	242	121	0.46	0.04607	9.800E-04	0.05235	0.0013	0.00824	0.00008	0.0027	0.00009	0.28	52.9	0.5	52	1	1	39	52.9	0.5	721	3.0
AC0702_30_049	190	99	0.47	0.04978	2.000E-03	0.05251	0.00232	0.00765	0.00007	0.00242	0.00002	0.28	49.1	0.5	52	2	185	90	49.1	0.5	708	3.1
AC0702_3_012	365	168	0.42	0.0492	3.020E-03	0.05122	0.00334	0.00755	0.00007	0.00239	0.00005	0.2	48.5	0.5	51	3	158	133	48.5	0.5	bdl	bdl
AC0702_24_041	617	295	0.43	0.04782	1.510E-03	0.05002	0.00186	0.00759	0.00008	0.00241	0.00003	0.4	48.7	0.5	50	2	90	69	48.7	0.5	bdl	bdl
AC0702_23_040	431	171	0.36	0.04703	1.260E-03	0.05286	0.0017	0.00815	0.00009	0.00259	0.00004	0.42	52.3	0.5	52	2	51	57	52.3	0.5	577	4.4
AC0702_21_038	343	184	0.49	0.04817	1.410E-03	0.05168	0.00176	0.00778	0.00008	0.00247	0.00003	0.35	50	0.5	51	2	108	66	50	0.5	bdl	bdl
AC0702_2_011	236	71	0.27	0.0495	2.370E-03	0.05541	0.00277	0.00812	0.00008	0.00257	0.00006	0.24	52.1	0.5	55	3	171	106	52.1	0.5	bdl	bdl
AC0702_19_034	496	223	0.41	0.04609	9.900E-04	0.04857	0.00124	0.00764	0.00008	0.00254	0.00012	0.35	49.1	0.5	48	1	2	39	49.1	0.5	bdl	bdl
AC0702_17_032	293	96	0.30	0.05345	3.230E-03	0.0556	0.00368	0.00754	0.00011	0.00236	0.00005	0.4	48.4	0.7	55	4	348	132	48.4	0.7	753	2.6
AC0702_14_027	75	27	0.33	0.05361	3.070E-03	0.06157	0.00374	0.00833	0.00011	0.00261	0.00004	0.26	53.5	0.7	61	4	355	125	53.5	0.7	729	2.9
AC0702_13_026	448	186	0.38	0.04903	1.640E-03	0.05151	0.00193	0.00762	0.00008	0.00241	0.00003	0.32	48.9	0.5	51	2	149	71	48.9	0.5	862	1.0
AC0702_12_025	359	171	0.43	0.04836	1.370E-03	0.05136	0.00164	0.0077	0.00007	0.00244	0.00002	0.31	49.5	0.4	51	2	117	60	49.5	0.4	685	3.4
AC0702_11_024	443	271	0.56	0.05389	1.560E-03	0.05898	0.0018	0.0077	0.00007	0.0034	0.00014	0.32	49.4	0.4	58	2	366	60	49.4	0.4	728	2.9
AC0702_1_010	107	55	0.47	0.05234	4.310E-03	0.0579	0.00504	0.00802	0.00011	0.00252	0.00006	0.28	51.5	0.7	57	5	300	171	51.5	0.7	710	3.1
Ac0705																						
AC0705_066	660	300	0.41	0.05027	1.590E-03	0.05328	0.00194	0.00769	0.00008	0.00242	0.00002	0.35	49.4	0.5	53	2	208	70	49.4	0.5	615	4.1
AC0705_064	708	291	0.37	0.04882	1.420E-03	0.05234	0.00158	0.00761	0.00006	0.0025	0.00004	0.27	48.9	0.4	52	2	139	64	48.9	0.4	749	2.7
AC0705_060	789	330	0.38	0.05022	5.130E-03	0.05328	0.00572	0.00769	0.0001	0.00243	0.00015	0.21	49.4	0.7	53	6	205	224	49.4	0.7	bdl	bdl
AC0705_059	741	339	0.42	0.04971	2.830E-03	0.05424	0.00313	0.00766	0.00007	0.00248	0.00004	0.16	49.2	0.4	54	3	181	133	49.2	0.4	614	4.1
AC0705_058	645	304	0.43	0.04792	1.100E-03	0.05237	0.00129	0.00778	0.00007	0.00254	0.00004	0.36	50	0.4	52	1	95	54	50	0.4	bdl	bdl
AC0705_056	862	415	0.44	0.04779	1.180E-03	0.05028	0.00153	0.00763	0.00008	0.00242	0.00003	0.43	49	0.5	50	1	89	57	49	0.5	615	4.1
AC0705_054	464	221	0.43	0.04803	1.400E-03	0.05141	0.0017	0.00776	0.00007	0.00246	0.00003	0.32	49.8	0.4	51	2	101	67	49.8	0.4	748	2.7
AC0705_053	615	280	0.41	0.04908	1.430E-03	0.0539	0.00183	0.00796	0.00008	0.00252	0.00003	0.36	51.1	0.5	53	2	152	69	51.1	0.5	715	3.1
AC0705_048	680	268	0.36	0.04623	1.290E-03	0.05179	0.00156	0.00783	0.00009	0.00267	0.00005	0.38	50.3	0.6	51	2	10	51	50.3	0.6	bdl	bdl
AC0705_044	382	146	0.35	0.05016	2.070E-03	0.05481	0.0024	0.00792	0.00007	0.0025	0.00003	0.27	50.9	0.5	54	2	202	89	50.9	0.5	bdl	bdl
AC0705_034	550	295	0.49	0.04869	3.320E-03	0.05107	0.00381	0.00761	0.00009	0.00241	0.00009	0.37	48.9	0.6	51	4	133	142	48.9	0.6	bdl	bdl
AC0705_030	758	299	0.36	0.04852	1.340E-03	0.05044	0.00182	0.00754	0.0001	0.00239	0.00003	0.53	48.4	0.6	50	2	125	60	48.4	0.6	624	4.1
AC0705_029	529	209	0.36	0.04789	1.250E-03	0.0521	0.00152	0.00789	0.00006	0.0025	0.00002	0.26	50.7	0.4	52	1	94	57	50.7	0.4	654	3.8
AC0705_027	558	173	0.28	0.04897	1.190E-03	0.05232	0.00151	0.00775	0.00008	0.00245	0.00003	0.42	49.8	0.5	52	1	146	58	49.8	0.5	bdl	bdl
AC0705_022	588	280	0.43	0.04766	1.600E-03	0.05018	0.00192	0.00764	0.00008	0.00242	0.00004	0.38	49	0.5	50	2	82	76	49	0.5	bdl	bdl
AC0705_020	669	293	0.40	0.04987	2.350E-03	0.05335	0.00286	0.00776	0.00011	0.00245	0.00004	0.37	49.8	0.7	53	3	189	109	49.8	0.7	760	2.5
AC0705_017	461	151	0.30	0.04827	1.300E-03	0.05182	0.00149	0.00776	0.00008	0.00273	0.00007	0.35	49.8	0.5	51	1	113	63	49.8	0.5	bdl	bdl
AC0705_009	573	284	0.45	0.04732	1.320E-03	0.04908	0.00164	0.00752	0.00008	0.00239	0.00004	0.38	48.3	0.5	49	2	65	61	48.3	0.5	bdl	bdl
AC0705_008	577	209	0.33	0.04875	1.330E-03	0.0507	0.00162	0.00754	0.00008	0.00239	0.00003	0.34	48.4	0.5	50	2	136	63	48.4	0.5	792	2.1
AC0705_038	786	331	0.38	0.05002	1.520E-03	0.05263	0.00194	0.00763	0.00009	0.00241	0.00003	0.45	49	0.6	52	2	196	69	49	0.6	666	3.6

(*continued*)

TABLE 3. U-Pb (*continued*)

				CORRECTED RATIOS†									CORRECTED AGES (Ma)									
	U (ppm)*	Th (ppm)*	Th/U	$^{207}Pb/^{206}Pb$	±1σ§	$^{207}Pb/^{235}U$	±1σ§	$^{206}Pb/^{238}U$	±1σ§	$^{208}Pb/^{232}Th$	±1σ§	Rho	$^{206}Pb/^{238}U$	±1σ	$^{207}Pb/^{235}U$	±1σ	$^{207}Pb/^{206}Pb$	±1σ	Best age (Ma)	±1σ	Ti-in T°C#	±1σ
Ac0707																						
AC0707_072	939	487	0.47	0.0478	1.620E-03	0.0515	0.002	0.00781	0.00009	0.00248	0.00004	0.38	50.2	0.6	51	2	90	71	50.2	0.6	583	4.4
AC0707_071	1038	407	0.36	0.04778	1.240E-03	0.05136	0.00141	0.00776	0.00007	0.00245	0.00006	0.33	49.8	0.4	51	1	88	56	49.8	0.4	822	1.7
AC0707_070	634	224	0.32	0.04749	1.950E-03	0.0528	0.00231	0.00806	0.00009	0.00256	0.00008	0.28	51.8	0.6	52	2	74	83	51.8	0.6	bdl	bdl
AC0707_068	780	358	0.42	0.04874	1.560E-03	0.05283	0.00179	0.00779	0.00009	0.00256	0.00006	0.33	50	0.6	52	2	135	69	50	0.6	692	3.4
AC0707_063	750	315	0.38	0.04723	1.370E-03	0.05187	0.00159	0.00792	0.00008	0.00251	0.00006	0.32	50.9	0.5	51	2	61	59	50.9	0.5	bdl	bdl
AC0707_052	926	377	0.37	0.04608	7.900E-04	0.05087	0.00111	0.00801	0.00008	0.00262	0.00009	0.34	51.4	0.5	50	1	2	31	51.4	0.5	bdl	bdl
AC0707_044	600	270	0.41	0.04871	1.750E-03	0.05182	0.00195	0.00779	0.00009	0.00255	0.00006	0.3	50	0.6	51	2	134	77	50	0.6	781	2.3
AC0707_041	852	430	0.46	0.04912	1.470E-03	0.05429	0.00172	0.00808	0.00008	0.0026	0.00005	0.33	51.9	0.5	54	2	154	65	51.9	0.5	bdl	bdl
AC0707_039	529	154	0.26	0.04622	1.250E-03	0.05169	0.00159	0.00811	0.00008	0.00259	0.00009	0.31	52.1	0.5	51	2	9	52	52.1	0.5	796	2.0
AC0707_034	352	133	0.34	0.04871	2.400E-03	0.05191	0.00277	0.00773	0.00009	0.00245	0.00005	0.24	49.6	0.6	51	3	134	107	49.6	0.6	bdl	bdl
AC0707_032	613	219	0.32	0.04918	1.920E-03	0.05125	0.00206	0.00775	0.00008	0.00264	0.00009	0.24	49.8	0.5	51	2	156	86	49.8	0.5	bdl	bdl
AC0707_028	633	234	0.34	0.04787	1.720E-03	0.04969	0.0021	0.00753	0.0001	0.00239	0.00004	0.38	48.4	0.6	49	2	93	77	48.4	0.6	752	2.7
AC0707_017	560	179	0.29	0.04834	1.620E-03	0.0512	0.00206	0.00768	0.0001	0.00243	0.00004	0.4	49.3	0.7	51	2	116	76	49.3	0.7	bdl	bdl
AC0707_015	409	176	0.39	0.04831	1.770E-03	0.05334	0.00226	0.00801	0.0001	0.00254	0.00004	0.33	51.4	0.6	53	2	114	82	51.4	0.6	bdl	bdl
AC0707_014	999	479	0.44	0.04757	1.470E-03	0.0522	0.00175	0.00777	0.0001	0.00259	0.00006	0.39	49.9	0.6	52	2	78	68	49.9	0.6	854	1.2
AC0707_064	960	382	0.36	0.04788	1.600E-03	0.05197	0.00209	0.00787	0.0001	0.0025	0.00004	0.43	50.5	0.7	51	2	93	71	50.5	0.7	777	2.3
AC0707_035	738	336	0.41	0.04896	2.350E-03	0.05327	0.0027	0.00788	0.00013	0.00246	0.00009	0.32	50.6	0.8	53	3	146	102	50.6	0.8	781	2.3
Ac0722																						
AC0722_071	932	448	0.44	0.04896	1.750E-03	0.05267	0.00216	0.0078	0.00009	0.00247	0.00003	0.36	50.1	0.6	52	2	146	81	50.1	0.6	776	2.3
AC0722_070	1171	515	0.40	0.04759	1.240E-03	0.04993	0.00141	0.00766	0.00008	0.0025	0.00006	0.39	49.2	0.5	49	1	79	58	49.2	0.5	823	1.7
AC0722_068	866	334	0.35	0.04722	2.780E-03	0.05121	0.00318	0.00787	0.00008	0.0025	0.00012	0.18	50.5	0.5	51	3	60	125	50.5	0.5	798	2.0
AC0722_066	808	325	0.37	0.04727	1.680E-03	0.05188	0.00206	0.00796	0.00009	0.00253	0.00006	0.29	51.1	0.5	51	2	63	75	51.1	0.5	751	2.7
AC0722_065	956	464	0.44	0.05133	1.640E-03	0.05597	0.00193	0.00783	0.0001	0.00248	0.00006	0.38	50.3	0.6	55	2	256	72	50.3	0.6	bdl	bdl
AC0722_064	430	146	0.31	0.05218	2.500E-03	0.05793	0.00304	0.00805	0.00011	0.00253	0.00004	0.29	51.7	0.7	57	3	293	108	51.7	0.7	bdl	bdl
AC0722_063	492	167	0.31	0.04959	2.190E-03	0.05383	0.00266	0.00787	0.00009	0.00249	0.00003	0.27	50.6	0.6	53	3	176	99	50.6	0.6	790	2.1
AC0722_060	1028	467	0.41	0.04775	2.500E-03	0.05031	0.00295	0.00764	0.00009	0.00243	0.00007	0.29	49.1	0.6	50	3	87	112	49.1	0.6	789	2.1
AC0722_054	779	537	0.63	0.04812	2.530E-03	0.053	0.00316	0.00799	0.0001	0.00253	0.00005	0.28	51.3	0.6	52	3	105	114	51.3	0.6	788	2.2
AC0722_051	822	298	0.33	0.0492	1.480E-03	0.05417	0.00177	0.00811	0.00011	0.00273	0.00008	0.39	52.1	0.7	54	2	157	68	52.1	0.7	853	1.2
AC0722_050	1246	700	0.51	0.04944	2.350E-03	0.05245	0.00285	0.00769	0.00009	0.00243	0.00003	0.28	49.4	0.6	52	3	169	107	49.4	0.6	644	3.9
AC0722_046	1321	596	0.41	0.04728	1.580E-03	0.05066	0.00226	0.00777	0.00014	0.00247	0.00006	0.49	49.9	0.9	50	2	64	73	49.9	0.9	759	2.6
AC0722_044	678	246	0.33	0.04902	3.500E-03	0.05329	0.00438	0.00788	0.00018	0.0025	0.00013	0.39	51	1	53	4	149	157	51	1	723	3.0
AC0722_040	705	305	0.39	0.05072	1.670E-03	0.05571	0.00198	0.00795	0.0001	0.00263	0.00007	0.38	51	0.6	55	2	228	76	51	0.6	bdl	bdl
AC0722_016	236	117	0.45	0.04902	2.950E-03	0.05481	0.00372	0.00811	0.00013	0.00257	0.00007	0.24	52.1	0.8	54	4	149	130	52.1	0.8	bdl	bdl
AC0722_014	537	221	0.37	0.04748	4.960E-03	0.05256	0.00581	0.00803	0.00014	0.00255	0.00026	0.15	51.5	0.9	52	6	74	204	51.5	0.9	bdl	bdl
AC0722_011	657	247	0.34	0.05175	3.620E-03	0.05593	0.00426	0.00784	0.0001	0.00246	0.00005	0.25	50.3	0.7	55	4	274	153	50.3	0.7	bdl	bdl
AC0722_069	1113	497	0.41	0.05325	3.770E-03	0.05716	0.00443	0.00778	0.00011	0.00244	0.00004	0.25	50	0.7	56	4	340	154	50	0.7	764	2.5
AC0722_056	407	140	0.31	0.05307	3.140E-03	0.05622	0.00365	0.00768	0.0001	0.00241	0.00003	0.26	49.3	0.7	56	4	332	129	49.3	0.7	753	2.6
AC0722_009	684	303	0.40	0.04918	4.260E-03	0.05327	0.00486	0.00786	0.0001	0.00249	0.00013	0.2	50.4	0.6	53	5	156	190	50.4	0.6	770	2.4
																			Average		739	3

*U and Th concetrations are calibrated relative to the analysis of NIST 612 trace element standard glass.
†Isotopic ratios are corrected relative to analysis of a standard zircon for mass bias and down-hole fractionation (see text for further explanations and the used zircon standards).
§Isotopic ratio errors are absolute and expressed at 1_ level. See text for further explanations. Apparent age errors are expressed at ±1σ.
#Ti-in zircon thermometry calculated according to Ferry and Watson (2007).

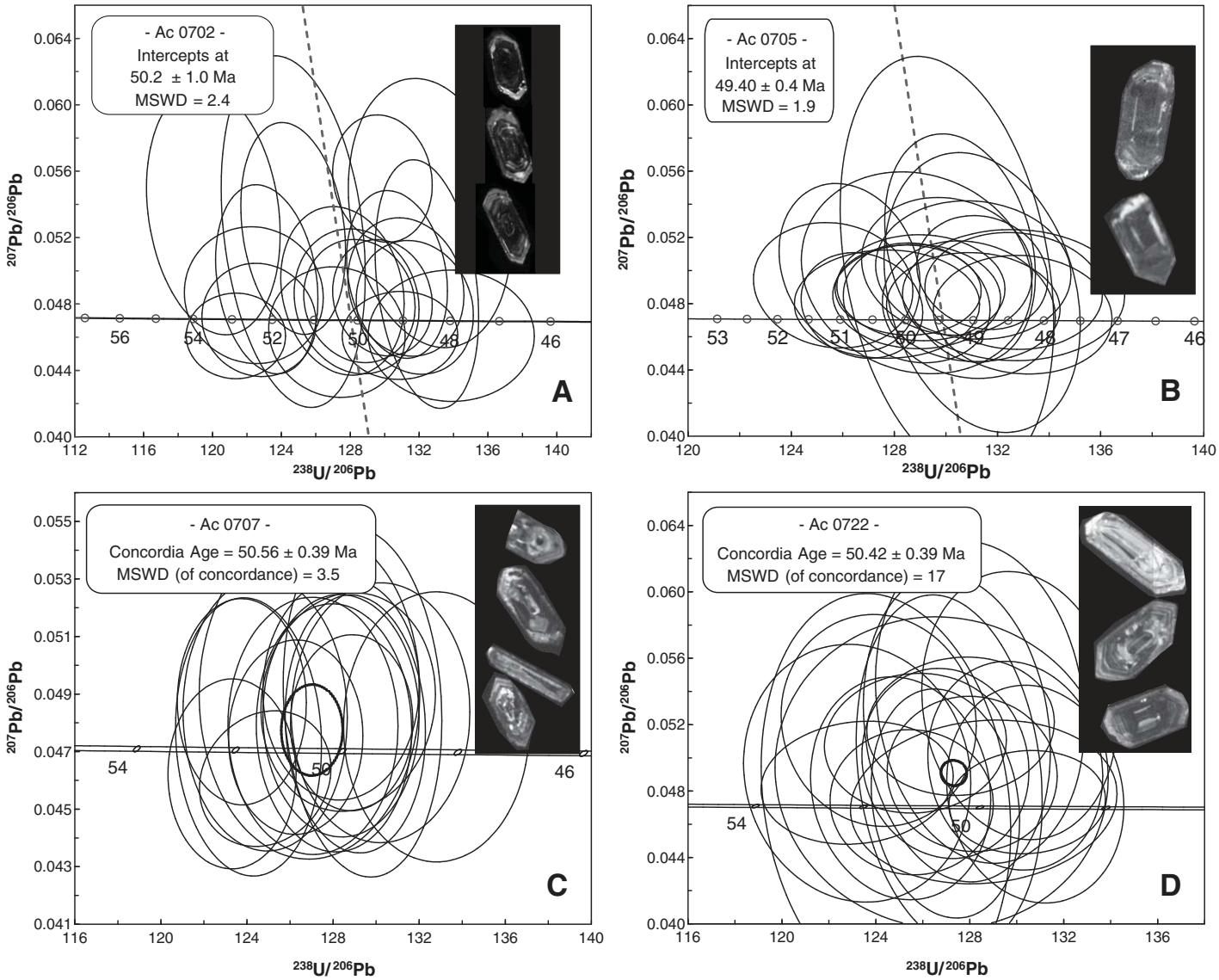

Figure 8. U-Pb concordia diagrams for samples of the Acapulco intrusion. Ellipses represent 2σ errors. Given errors in calculated ages are 2σ. MSWD—mean square of weighted deviates. Ninety-five percent of confidence and decay-constant errors included. Some representative cathodoluminescence images of selected zircons are also represented. Width of the black rectangles is 200 µm. A—Rapakivi granite, sample Ac 0702; B—Quartz syenite, sample Ac 0705; C—Rapakivi granite, sample Ac 0707; D—Rapakivi granite, sample Ac 0722.

(Fig. 4D), suggesting Fl crystallized in a later stage at lower magmatic water contents. This behavior has been explained as the entrapment of halogens in the silicic dry magma until reaching the saturation point, which usually occurs after the final crystallization of hydrous phases (Kilinc and Burnham, 1972; Frost and Frost, 1997). On the other hand, fluorine, along with Kfs, reduces the viscosity of the magma, affects the diffusion rate in Na-K system, and decreases the melting point of feldspars (Giordano et al., 2004). As a result, Kfs crystals exsolve their molar albite fraction developing the observed perthitic textures (Snow and Kidman, 1991). Thus, we consider that fluorine played a key role in the development of the characteristic mineralogy in the Acapulco intrusion, as also reported in other felsic magmatic systems (e.g., Agangi et al., 2010).

It is also known that Aln can control LREE content (e.g., Ce and La) and Th as well in granitic magmas (Deer et al., 1986; Gieré and Sorensen, 2004; Hoshino et al., 2005). Beyond its effect in the trace-element distribution, the occurrence of Aln in metaluminous rocks with high-aluminum content suggests that crystallization of this magma took place between 600 and 800 °C (Chesner and Ettlinger, 1989; Gieré and Sorensen, 2004), which is in accordance with our thermometric determinations of 700–730 °C.

Development of the Rapakivi Texture

The origin of Kfs crystals immersed in a Pl mantle, better known as rapakivi texture, has been under debate for several decades since it was first described (Stimac and Wark, 1992, and references therein). Sensu stricto, a rapakivi texture is defined as ovoid-shaped Kfs crystals surrounded by Pl rims with an average composition of $Ab_{90–70}$. In the case of the Acapulco granite, euhedral Kfs crystals are rimmed by albitic Pl

TABLE 4. EMPA RESULTS WITH THERMOMETRY AND BAROMETRY

Sample	Ac0703		Ac0707					Ac0703c	
Mineral	Hbl	Hbl	Hbl	Pl	Hbl	Hbl	Pl	Hbl	Pl
SiO_2	43.48	43.55	42.63	66.68	43.56	42.78	65.91	43.43	64.49
TiO_2	1.68	1.60	1.22	0.04	1.59	1.15	0.03	1.73	0.01
Al_2O_3	7.35	7.20	6.88	20.60	6.75	6.84	20.52	6.72	22.41
FeO	24.75	24.57	27.14	0.12	26.58	27.23	0.33	24.97	0.06
MnO	0.92	1.00	1.16	0.00	1.08	0.99	0.01	0.86	0.02
Cr_2O_3	0.01	0.00	0.01	0.02	0.00	0.01	0.00	0.01	0.02
MgO	6.51	6.28	4.92	0.00	5.55	5.04	0.01	6.68	0.01
CaO	10.13	10.21	10.11	1.57	9.91	10.24	1.65	9.91	3.51
Na_2O	1.98	1.91	2.13	10.61	2.40	2.16	10.77	1.97	9.68
K_2O	0.88	0.88	1.08	0.65	0.86	1.13	0.49	0.83	0.48
Total	97.69	97.18	97.27	100.30	98.27	97.57	99.71	97.12	100.69
Feldspar proportion (%)									
Ab				89.11			89.72		81.08
An				7.22			7.61		16.12
Or				3.54			2.71		2.65
Cations									
Si	6.80	6.84	6.82	2.93	6.85	6.82	2.91	6.84	2.83
Ti	0.20	0.19	0.15	0.00	0.19	0.14	0.00	0.21	0.00
Al	1.36	1.33	1.30	1.07	1.25	1.29	1.07	1.25	1.16
Fe	3.24	3.23	3.63	0.00	3.49	3.63	0.01	3.29	0.00
Mn	0.12	0.13	0.16	0.00	0.14	0.13	0.00	0.11	0.00
Cr	0.00	0.00	0.00	0.00	0.00	0.00	0.00	0.00	0.00
Mg	1.52	1.47	1.17	0.00	1.30	1.20	0.00	1.57	0.00
Ca	1.70	1.72	1.73	0.07	1.67	1.75	0.08	1.67	0.17
Na	0.60	0.58	0.66	0.90	0.73	0.67	0.92	0.60	0.82
K	0.17	0.18	0.22	0.04	0.17	0.23	0.03	0.17	0.03
Total	38.71	38.68	38.83	13.01	38.79	38.85	13.03	38.71	13.01
Temperature (°C)	735.75		695.25		694.00*	692.75		736.75	
Pressure (kbar)	2.84	2.70	2.32		2.08	2.25		2.18	
Depth (km)	10.73	10.21	8.76		7.84	8.50		8.24	

Note: Electron microprobe analysis in hornblende-plagioclase association. Structural formulae were calculated on the basis of 23 oxygens and 13 cations for hornblende (Hbl), and 8 oxygens and 5 cations for plagioclase (Pl). Thermometric determinations were obtained with Hbl+Pl B-thermometer (edenite-richterite) from Holland and Blundy (1994). Pressures were calculated using Al_{tot}-in-Hornblende barometer from Anderson and Smith (1996). Depths were calculated assuming lithostatic pressure using $h = P(\rho g)^{-1}$ were h is depth, P is the pressure, ρ is the mean density (2.7 g cm^{-3}), and g is the acceleration due to gravity (9.8 m s^{-2}).

*Average calculated temperature for sample Ac0707.

giving place to a pseudo-rapakivi or rapakivi texture sensu lato (Dempster et al., 1994). The metaluminous to peraluminous character of the Acapulco granite, with pyroxene relicts and general crystallization temperatures around 700 °C, corresponds to a typical rapakivi granite, which is subsaturated in water and emplaced at a maximum depth of 10 km (Haapala and Ramö, 1990; Emslie, 1991; Stimac and Wark, 1992).

Different models have been proposed for the origin of the rapakivi texture. In general, two interpretations dominate: (1) a magmatic origin and (2) a subsolidus origin (Dempster et al., 1994). The magmatic process invokes immiscibility between two types of melts, metasomatic replacement, magma mixing or assimilation of mafic rocks, and fluid saturated magma degassification (Stimac and Wark, 1992; Dempster et al., 1994; Ramö and Haapala, 1996; Frost and Frost, 1997; Calzia and Ramö, 2005). Although there are many inconsistencies in those models, and considering that the rapakivi granites represent large batholiths, such mechanisms seem to be unrealistic due to the thermal and volumetric implications (Dempster et al., 1994). On the other hand, what has been called the subsolvus mechanism can present some problems to exsolve sodic plagioclase from alkaline feldspar due to the low diffusion rate of alkalis in the Kfs (Snow and Kidman, 1991; Dempster et al., 1994).

Therefore, we propose a model for the Acapulco granite rapakivi texture based on our petrologic, mineral, and chemical observations. At the early stage of crystallization, Kfs crystals were stable and well developed (Fig. 9A). Later, during the initial stage of crystallization of the hydrous phases, the concentration of halogens increased. Fluorine saturation favored Kfs instability, forcing it to exsolve its Pl molar fraction, mainly of oligoclase composition, developing perthites and further lamellae textures (Figs. 9B and 9C). Albitic plagioclase was exsolved later, forming the phenocrystic rims of the rapakivi texture (Fig. 9D).

Is the Acapulco Intrusion Part of an A-Type, Alkaline Magmatic Pulse in Southern Mexico?

Since the first description of the Acapulco granite by De Cserna (1965), this pluton has been considered part of an alkaline magmatic event within the coastal batholithic belt. There are many factors that support this interpretation, including the rapakivi texture, Fl occurrence, and pyroxene relicts. It is not unusual to associate alkaline rocks with continental rift and post-collision magmatism, because such rocks show mantle-like isotopic signatures and hypersolvus, as well as the typical rapakivi textures that normally form at shallow depths (Anderson, 1983; Kemp and Hawkesworth, 2004). This evolution is not congruent, however, with the geological setting of the coastal batholithic belt that has been interpreted as a continental magmatic arc (Schaaf et al., 1995).

As we established earlier, Ca, Ba, Sr, and Eu depletion was controlled by fractional crystallization in equilibrium with Pl (Fig. 10A). Such effect could produce incompatible element enrichment (Kemp and Hawkesworth, 2004), but the less evolved unit of the intrusive (diorites) still maintains chemical characteristics of arc-related rocks (Fig. 10A). The incompatible elements enrichment is considered a diagnostic feature for A-type granites together with extremely high Zn content (>>80 ppm) combined with high Ga/Al ratios (Collins et al., 1982; Whalen et al., 1987). Samples belonging to the Acapulco intrusion are not within this range, though their (Ga/Al) × 10^4 ratios are as high as 3.32, a feature that may have resulted from fractional crystallization of plagioclase (Kemp and Hawkesworth, 2004). This behavior may be a convergence between highly fractionated metaluminous I-type granites and A-type

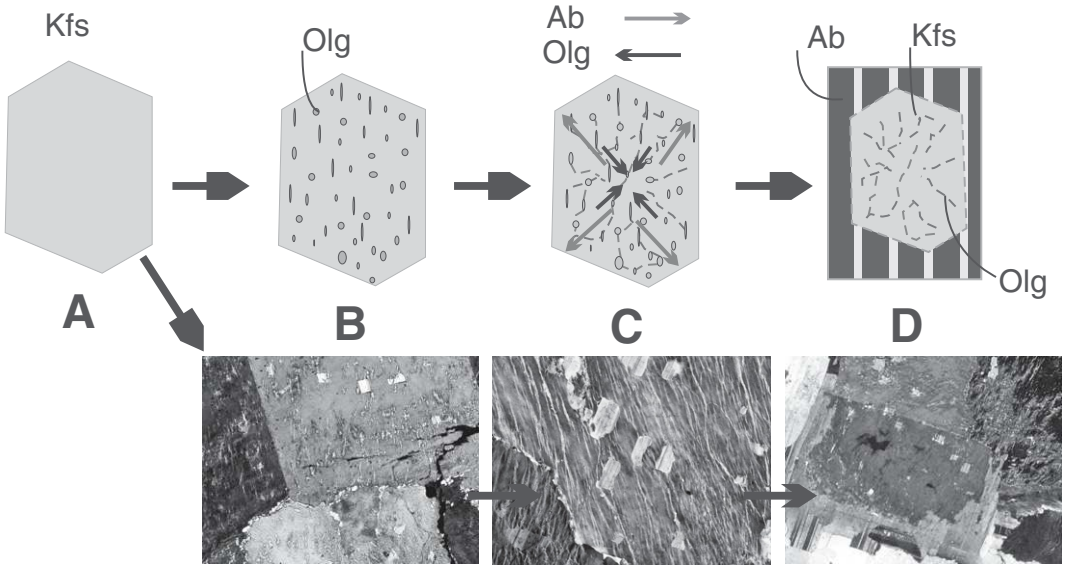

Figure 9. Schematic development of the rapakivi texture with photomicrographs of different stages of evolution (see text for explanation).

granites, as is shown in Figure 10B. Furthermore, by comparing the Eu anomaly (Eu/Eu*) with Th content, it is clear that the Acapulco intrusion belongs to a suite of I-type granites according to Eby (1992) (Fig. 10C). Even though all these classifications are considered empirical, we believe that they can be applied in order to understand graphically those chemical differences between the A-type granites and the Acapulco intrusion (Fig. 10).

Role of Crustal Assimilation

The geological and analytical data provided in this paper suggest that the Acapulco granite was emplaced during a magmatic stage related to the Laramide subduction process. This interpretation differs from the traditional idea of an alternative tectonic scenario related to intraplate magmatism (e.g., Morán-Zenteno et al., 1996). The high Pb/Ce (0.06–0.27) and Th/Nd (0.07–1.38) ratios of the Acapulco granite are not typical of intraplate magmatism and suggest either a crustal or subducted sediment contribution in a subduction setting. Yet the relatively constant Nd and Sr isotopic compositions at variable Th/Nd and $^{87}Sr/^{86}Sr$ ratios are inconsistent with sediment additions, because all these elements are similarly mobile in the subduction flux and thus should enrich the source at the same time (Gómez-Tuena, et al., 2007). Crustal contamination will modify the isotopes concurrently with fractionation only if a large isotopic contrast exists between the primitive magma and the contaminant. Since the only significant isotopic distinction between the Acapulco granite and the local basement (Xolapa Complex) is observed in the Sr isotopes (Fig. 7), and especially in its micas, the effects of crustal contamination can be better constrained using this isotopic system (Fig. 10D). Thus, we conclude that contamination with the mica-rich lithology of the Xolapa Complex is responsible for the radiogenic Sr isotopic compositions observed in the most evolved syenites. Since mica does not incorporate Nd or Pb in significant quantities (Bebout et al., 2007), these isotopic systems will remain undisturbed during assimilation.

The origin of the high fluorine concentrations, permitting the crystallization of fluorite from the magma remains uncertain. The geochemical behavior of fluorine in subduction-related settings is generally considered to be conservative, because only ~4% of it is recycled by dehydration of secondary amphibole carried by the subducted oceanic slab and released into the overlying mantle wedge (Ito et al., 1983; Straub and Layne, 2003). Thus, the excess fluorine in the Acapulco intrusion cannot be attributed to subduction-related processes alone. The variation in radiogenic Sr tends toward the composition of white mica (e.g., muscovite, Fig. 10D), which is contained in the older metasediments of the Xolapa Complex (>130 Ma, e.g., Morán-Zenteno, 1992; Solari et al., 2007). Thus, it is likely that the contamination of the Acapulco intrusion (in particular the quartz syenites) resulted from the interaction between released fluids from the host rocks and the granitic magmas. Such fluorine-enriched fluids can be explained by mica (muscovite) dehydration from the surrounding metasediments from the Xolapa Complex at temperatures above 700 °C (e.g., Guggenheim et al., 1987). Furthermore, this process could provide an explanation for the presence and origin of the fluorine-rich fluids in the Acapulco magmatic system.

The Evolution of the Acapulco Intrusion and Its Tectonic Implications in Post-Laramidic Magmatism

The thermobarometric results obtained in this paper (e.g., 10 km maximum depth) allows the construction of an exhumation curve (Fig. 11A), which has been adjusted with those estimations for the Xolapa Complex for the past 20 Ma (~3.6 km depth) based on (U-Th)/He thermochronology (Ducea et al., 2004b). We can establish two different exhumation rates that consist of a first period with a moderate rate of 0.21 km/m.y. and a second period of slower exhumation rate of 0.18 km/m.y. (Fig. 11A; Ducea et al., 2004b). These estimations differ from those obtained by Morán-Zenteno et al. (1996), who considered an emplacement depth between 13 and 20 km, calculating a constant exhumation rate of 0.44 km/m.y. before 20 Ma. The nearby younger and nondeformed plutons of Tierra Colorada, Xaltianguis, and San Juan del Reparo, show crystallization ages between 32 and 34 Ma (Herrmann et al., 1994; Ducea et al., 2004a; Hernández-Pineda, 2006). According to their chemistry, mineralogy and textural characteristics were probably emplaced at a maximum depth of ~6 km (Fig. 11A).

The Paleocene magmatic event in southern Mexico is still poorly understood due to the scarcity of outcrops (Morán-Zenteno et al., 2007). However, recent U-Pb zircon geochronological data from the coastal batholithic belt (e.g., Ducea et al., 2004a; Solari et al., 2007; Martini, 2008; Pérez-Gutiérrez et al., 2009; Valencia et al., 2009; and this paper), confirm the occurrence of a regional magmatic episode between 50 and 60 Ma for the central portion along the

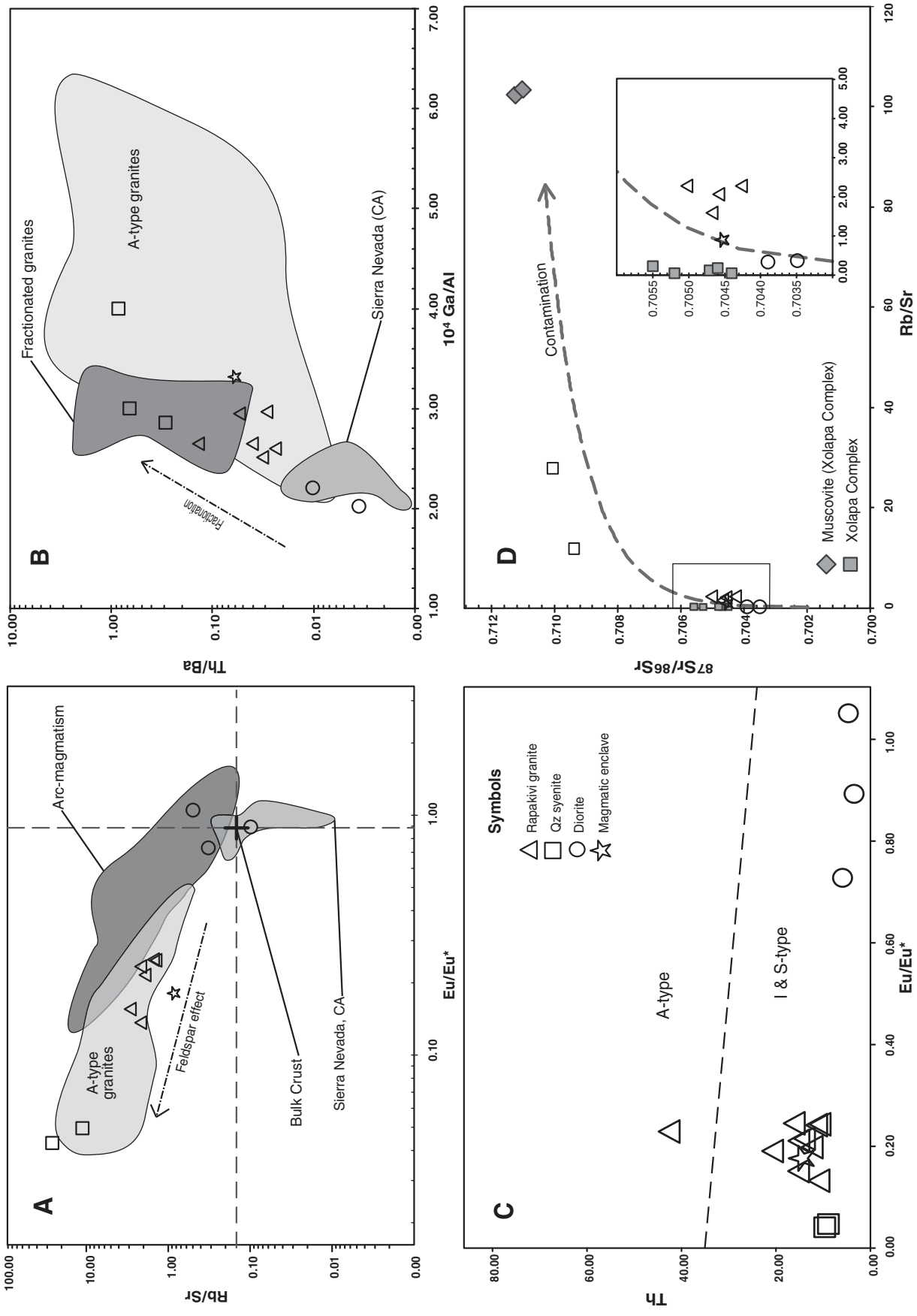

Figure 10. Variation diagrams for selected trace elements and Sr isotopes: (A) Eu/Eu* versus Rb/Sr showing the effect of fractionation of feldspars; (B) 10^4Ga/Al versus Th/Ba with the overlapped field for A-type and highly fractionated granites; (C) typology Eu/Eu* versus Th discrimination diagram after Eby (1992); (D) contamination from muscovites of the wallrock metasedimentary sequence from the Xolapa Complex using Rb/Sr versus $^{87}Sr/^{86}Sr$. Data from: Sierra Nevada (California [CA]) (North American volcanic and intrusive rocks [NAVDAT]: Walker et al., 2006); A-type granites (Whalen et al., 1987); arc-magmatism (geochemistry of rocks of the oceans and continents [GEOROC]: Nohl and Sarbas, 1999); bulk crust (Kemp and Hawkesworth, 2004); fractionated granites (Whalen et al., 1987); Xolapa Complex (Morán-Zenteno, 1992; Herrmann et al., 1994; Pérez-Gutiérrez et al., 2009); and muscovite from Xolapa Complex (Morán-Zenteno, 1992).

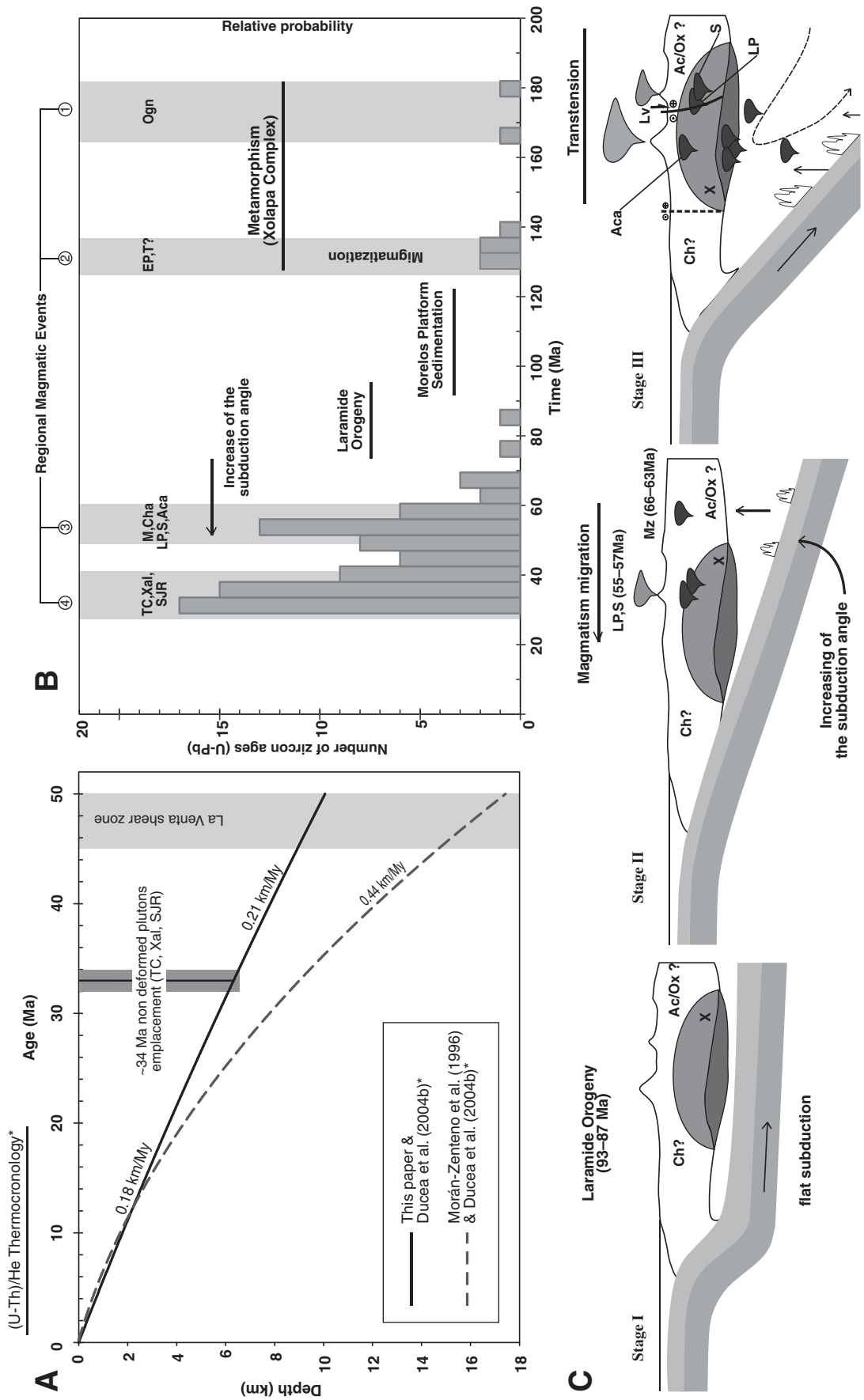

Figure 11. (A) Different proposed exhumation trajectories of the Acapulco intrusion. The trajectories and exhumation rates are calculated with the barometric determinations presented in this paper and published data. (U-Th)/He thermochronology: Ducea et al. (2004b); previous geobarometry: Morán-Zenteno et al. (1996); young and nondeformed plutons: Herrmann et al. (1994), Ducea et al. (2004a), and Hernández-Pineda (2006); (B) identification of the tectonic and magmatic events along the coastal zone in the Guerrero State (southern Mexico), based on the relative probability of U-Pb zircon ages: geochronological data from this paper together with Guerrero-García et al. (1978), Herrmann et al. (1994), Ducea et al. (2004a), Hernández-Pineda (2006), Solari et al. (2007), Pérez-Gutiérrez et al. (2009), and Valencia et al. (2009); and (C) schematic cartoon showing the tectonic evolution and migration of the post-Laramide magmatism in three stages (see text for explanation). Abbreviations: TC—Tierra Colorada; Xal—Xaltianguis; SJR—San Juan del Reparo; M—Mezcala; Cha—Chacalapa; LP—Las Piñas; S—El Salitre; Aca—Acapulco; EP—El Pozuelo; T—Tamuchis; Ogn—Ortogneisses; Ch—Chortis block; Ac/Ox—Acatlán-Oaxacan Complexes; X—Xolapa Complex; Lv—La Venta shear zone.

coast (e.g., between Zihuatanejo and Acapulco), which characterizes a post-Laramide magmatic event in this area of southern Mexico (Fig. 11B).

After cessation of the Laramide orogeny in southern Mexico, which, according to Cerca et al. (2007) and Solari et al. (2007), was characterized by flat subduction, the slab increased the angle of subduction producing a N-S migration toward the coast from 68 to 50 Ma in the Mezcala-Acapulco sector (Meza-Figueroa et al., 2003; Ducea et al., 2004a; Solari et al., 2007). This rearrangement in the subduction geometry increased the geothermic gradient giving place to the 60–50 Ma magmatic pulse (Fig. 11C).

The ascent and emplacement of the magmas from the Acapulco intrusion may have occurred during the extensional deformation represented near the studied area by La Venta shear zone, ~30 km N from Acapulco, dated at 45–50 Ma (Solari et al., 2007) (Figs. 11A and 11C). This extensional event has been associated either with an oblique convergence between the Farallon and North American plates or with the separation of the Chortís block from southern Mexico (Herrmann et al., 1994; Schaaf et al., 1995; Morán-Zenteno et al., 1996). Such mechanism is well documented worldwide and associated with the generation of space that allows the ascent and emplacement of granitic magmas (Hutton et al., 1990; Vigneresse, 1995a, 1995b; Petford et al., 2000).

CONCLUSIONS

We presented geologic, geochemical, geochronologic, and thermobarometric data for the Acapulco intrusion as an example of post-Laramide magmatism in southern Mexico. Based on our results and those previously published, we propose a tectono-magmatic evolution summarized in Figures 11B and 11C in which the ~50 Ma Acapulco intrusion is part of the post-Laramide magmatic event originated through the increment in the angle of subduction, which favors the north to south migration of the magmatism in the area. We also document the contribution of radiogenic Sr- and F-saturated fluid conditions recorded in the metaluminous-peraluminous Acapulco intrusion as a contamination feature of muscovite-bearing metasediments of the Xolapa Complex. This process occurred due to the remobilization during high-temperature emplacement of the Acapulco body. Furthermore, we propose a model for development of the rapakivi texture originated by the fractional crystallization of plagioclase, combined with high-fluorine fugacity. Finally, the combination of previously available data and those presented here allow us to establish two exhumation rates for the Acapulco intrusion: the first one of 0.21 km/m.y. since its emplacement at ~10 km of depth, which is followed by a second stage of 0.18 km/m.y. starting in the Miocene, ~20 Ma (Ducea et al., 2004b).

As a whole, the post-Laramide plutonism in southern Mexico, characterized by the absence of penetrative deformation, occurred in a quite long-lasting event from the latest Paleocene (e.g., Solari et al., 2007) to the earliest Oligocene (e.g., Schaaf et al., 1995; Ducea et al., 2004a). Thanks to our current work, the Acapulco intrusive is now one of the best characterized examples of this widespread plutonic event, which constitutes the eroded roots of the late Eocene to Miocene volcanic arc of Sierra Madre del Sur (e.g., Morán-Zenteno et al. 2007).

ACKNOWLEDGMENTS

Fruitful discussions with F. Ortega-Gutiérrez, D. Morán-Zenteno, C. Mattinson, and F. Jenner allowed clarification of several aspects in this research. This paper benefited from funds granted to LAS from Consejo Nacional de Ciencia y Tecnologia (CONACyT) (54559 and J-39783) and PAPIIT IN101407. GAHP wants to thank J.G. Liou, W.G. Ernst, and U. Martens, from Stanford University, for all their support and advice during his stay in the 2008 winter quarter. GAHP was supported during his Master's thesis studies at UNAM by a CONACyT scholarship. We wish to thank R. Jones for assistance at the electron microprobe analysis laboratory at Stanford University. We would also thank P. Schaaf, G. Solís-Pichardo, J.J. Morales, M.S. Hernández-Bernal, and T. Hernández-Treviño from LUGIS for assistance and their participation during isotope analytical work and data acquisition. J. Callejas Moreno and R. Hernández Ordoñez are thanked for their assistance and company during fieldwork. We appreciate comments and reviews from the editor C. Frost and M. Valencia-Moreno, T. Toulkeridis, and an anonymous reviewer that helped to improve the manuscript.

REFERENCES CITED

Agangi, A., Kamenetsky, V., and McPhie, J., 2010, The role of fluorine in the concentration and transport of lithophile trace elements in felsic magmas: Insights from the Gawler Range volcanics, South Australia: Chemical Geology, v. 273, p. 314–325, doi:10.1016/j.chemgeo.2010.03.008.

Anderson, J.L., 1983, Proterozoic anorogenic granite plutonism of North America: Geological Society of America Memoir 161, p. 133–154.

Anderson, J.L., 1996, Status of thermobarometry in granitic batholiths: Transactions of the Royal Society of Edinburgh, Earth Sciences, v. 87, p. 125–138.

Anderson, J.L., and Smith, D.R., 1995, The effect of temperature and oxygen fugacity on Al-in-hornblende barometry: The American Mineralogist, v. 80, p. 549–559.

Armstrong, J.T., 1988, Quantitative analysis of silicate and oxide minerals: Comparison of Monte Carlo, ZAF, and Phi-Rho-Z procedures, *in* Newbury, D.E., ed., Analysis Microbeam: San Francisco, California, San Francisco Press, p. 239–246.

Bebout, G.R., Bebout A.E., and Graham, C.E., 2007, Cycling of B, Li, and LILE (K, Cs, Rb, Ba, Sr) into subduction zones: SIMS evidence from micas in high-P/T metasedimentary rocks: Chemical Geology, v. 239, p. 284.

Calzia, J.P., and Rämö, O.T., 2005, Miocene rapakivi granites in the southern Death Valley region, California, USA: Earth-Science Reviews, v. 73, p. 221–243, doi:10.1016/j.earscirev.2005.07.006.

Campa, M.F., and Coney, P.J., 1983, Tectono-stratigraphic terranes and mineral resource distributions in Mexico: Canadian Journal of Earth Sciences, v. 20, p. 1040–1051, doi:10.1139/e83-094.

Centeno-García, E., Guerrero-Suastegui, M., and Talavera-Mendoza, O., 2008, The Guerrero composite terrane of western Mexico: Collision and subsequent rifting in a supra-subduction zone, *in* Draut, A., Clift, P.D., and Scholl, D.W., eds., Formation and Applications of the Sedimentary Record in Arc Collision Zones: Geological Society of America Special Paper 436, p. 279–308.

Cerca, M., Ferrari, L., López-Martínez, M., Martiny, B., and Iriondo, A., 2007, Late Cretaceous shortening and early Tertiary shearing in the central Sierra Madre del Sur, southern Mexico: Insights into the evolution of the Caribbean–North American plate interaction: Tectonics, v. 26, TC3007, p. 34, doi:10.1029/2006TC001981.

Chesner, C.A., and Ettlinger, A.D., 1989, Composition of volcanic allanite from the Toba Tuffs, Sumatra, Indonesia: The American Mineralogist, v. 74, p. 750.

Collins, W.J., Beams, S.D., White, A.J.R., and Chappell, B.W., 1982, Nature and origin of A-type granites with particular reference to southeastern Australia: Contributions to Mineralogy and Petrology, v. 80, p. 189–200, doi:10.1007/BF00374895.

De Cserna, Z., 1965, Reconocimiento geológico en la Sierra Madre del Sur de México, entre Chilpancingo y Acapulco, Estado de Guerrero: Universidad Nacional Autónoma de México, Instituto de Geología: Boletin (Instituto de Estudios de Poblacion y Desarrollo, Dominican Republic), v. 62, p. 77.

Deer, W.A., Howie, R.A., and Zussman, J., 1986, An Introduction to the Rock-Forming Minerals, 2nd edition: Pearson-Prentice Hall, 369 p.

Dempster, T.J., Jenkin, G.R.T., and Rogers, G., 1994, The origin of rapakivi texture: Journal of Petrology, v. 35, p. 963.

Dickinson, W.R., and Lawton, T.F., 2001, Carboniferous to Cretaceous assembly and fragmentation of Mexico: Geological Society of America Bulletin, v. 113, p. 1142–1160, doi:10.1130/0016-7606(2001)113<1142:CTCAAF>2.0.CO;2.

Ducea, M.N., Gehrels, G.E., Shoemaker, S., Ruiz, J., and Valencia, V.A., 2004a, Geologic evolution of the Xolapa Complex, southern Mexico: Evidence from U-Pb zircon geochronology: Geological Society of America Bulletin, v. 116, p. 1016, doi:10.1130/B25467.1.

Ducea, M.N., Valencia, V.A., Shoemaker, S., Reiners, P.W., DeCelles, P.G., Campa, M.F., Morán-Zenteno, D., and Ruiz, J., 2004b, Rates of sediment recycling beneath the Acapulco trench: Constraints from (U-Th)/He thermochronology: Journal of Geophysical Research, v. 109, p. B09404, doi:10.1029/2004JB003112.

Eby, G.N., 1992, Chemical subdivision of the A-type granitoids: Petrogenetic and tectonic implications: Geology, v. 20, p. 641, doi:10.1130/0091-7613(1992)020<0641:CSOTAT>2.3.CO;2.

Emslie, R.F., 1991, Granitoids of rapakivi granite-anorthosite and related associations: Precambrian Research, v. 51, p. 173–192, doi:10.1016/0301-9268(91)90100-O.

Engebretson, D.C., Cox, A., and Gordon, R.G., 1985, Relative motions between oceanic and continental plates in the Pacific basin: Geological Society of America Special Paper 206, 64 p.

Ferry, J.M., and Watson, E.B., 2007, New thermodynamic models and revised calibrations for the Ti-in-zircon and Zr-in-rutile thermometers: Contributions to Mineralogy and Petrology, v. 154, no. 4, p. 429–437, doi:10.1007/s00410-007-0201-0.

Frost, C.D., and Frost, R., 1997, Reduced rapakivi-type granites: The tholeiite connection: Geology, v. 25, p. 647, doi:10.1130/0091-7613(1997)025<0647:RRTGTT>2.3.CO;2.

Gieré, R., and Sorensen, S.S., 2004, Allanite and other REE-rich epidote-group minerals: Reviews in Mineralogy and Geochemistry, v. 56, p. 431, doi:10.2138/gsrmg.56.1.431.

Giordano, D., Romano, C., Dingwell, D.B., Poe, D., and Behrens, H., 2004, The combined effects of water and fluorine on the viscosity of silicic magmas: Geochimica et Cosmochimica Acta, v. 68, p. 5159–5168, doi:10.1016/j.gca.2004.08.012.

Gómez-Tuena, A., Langmuir, C.H., Goldstein, S.L., Straub, S.M., and Ortega-Gutiérrez, F., 2007, Geochemical evidence for slab melting in the Transmexican Volcanic Belt: Journal of Petrology, v. 48, p. 537–562, doi:10.1093/petrology/egl071.

Guerrero-García, J.C., Silver, L.T., and Anderson, T.H., 1978, Estudios geocronológicos en el Complejo Xolapa: Boletín de la Sociedad Geológica Mexicana, v. 39, p. 22–23.

Guggenheim, S., Chang, Y.-H., and Koster van Groos, A.F., 1987, Muscovite dehydroxylation: High-temperature studies: The American Mineralogist, v. 72, p. 537–550.

Haapala, I., and Rämö, O.T., 1990, Petrogenesis of the Proterozoic rapakivi granites of Finland: Geological Society of America Special Paper, v. 246, p. 275–286.

Hernández-Bernal, M.S., and Morán-Zenteno, D.J., 1996, Origin of the Río Verde batholith, southern Mexico, as inferred from is geochemical characteristics: International Geology Review, v. 38, p. 361–373, doi:10.1080/00206819709465340.

Hernández-Pineda, G.A., 2006, Geocronología y geoquímica de granitoides en el área de Tierra Colorada, Guerrero: México [B.S. thesis]: Universidad Nacional Autónoma de México, 85 p.

Herrmann, U.R., Nelson, B.K., and Ratschbacher, L., 1994, The origin of a terrane: U/Pb zircon geochronology and tectonic evolution of the Xolapa Complex (southern Mexico): Tectonics, v. 13, p. 455–474, doi:10.1029/93TC02465.

Holland, T., and Blundy, J., 1994, Non-ideal interactions in calcic amphiboles and their bearing on amphibole-plagioclase thermometry: Contributions to Mineralogy and Petrology, v. 116, p. 433–447, doi:10.1007/BF00310910.

Hoshino, M., Kimata, M., Nishida, N., Kyono, A., Shimizu, M., and Takizawa, S., 2005, The chemistry of allanite from the Daibosatsu Pass, Yamanashi, Japan: Mineralogical Magazine, v. 69, p. 403, doi:10.1180/0026461056940259.

Hutton, D.H.W., Dempster, T.J., Brown, P.E., and Becker, S.D., 1990, A new mechanism of granite emplacement: Intrusion in active extensional shear zones: Nature, v. 343, p. 452–455, doi:10.1038/343452a0.

Irvine, T.N., and Baragar, W.R.A., 1971, A guide to the chemical classification of the common volcanic rocks: Canadian Journal of Earth Sciences, v. 8, p. 523–548, doi:10.1139/e71-055.

Ito, E., Harris, D., and Anderson, A.T., 1983, Alteration of oceanic crust and geologic cycling of chlorine ad water: Geochimica et Cosmochimica Acta, v. 47, p. 1613–1624, doi:10.1016/0016-7037(83)90188-6.

Ito, E., White, W.M., and Gopel, C., 1987, The O, Sr, Nd and Pb isotope geochemistry of MORB: Chemical Geology, v. 62, p. 157–176, doi:10.1016/0009-2541(87)90083-0.

Johnson, M.C., and Rutherford, M.J., 1989, Experimental calibration of the aluminum-in-hornblende geobarometer with application to Long Valley caldera (California) volcanic rocks: Geology, v. 17, p. 837, doi:10.1130/0091-7613(1989)017<0837:ECOTAI>2.3.CO;2.

Kemp, A.I.S., and Hawkesworth, C.J., 2004, Granitic Perspectives on the Generation and Secular Evolution of the Continental Crust, *in* Rudnick, R.L., ed., Treatise on Geochemistry, v. 3, The Crust: Amsterdam, Elsevier, p. 349–410.

Keppie, J.D., 2004, Terranes of Mexico revisited: A 1.3 billion year odyssey: International Geology Review, v. 46, p. 765–794, doi:10.2747/0020-6814.46.9.765.

Keppie, J.D., and Morán-Zenteno, D.J., 2005, Tectonic implications of alternative Cenozoic reconstructions of southern Mexico and the Chortis block: International Geology Review, v. 47, p. 473–491, doi:10.2747/0020-6814.47.5.473.

Keppie, J.D., Morán-Zenteno, D., Martiny, B., and González-Torres, E., 2009, Synchronous 29–19 Ma arc hiatus, exhumation and subduction of forearc in southwestern Mexico, *in* James, K., Lorente, M.A., and Pindell, J., eds., Origin and Evolution of the Caribbean Plate: The Geological Society of London, Special Publication 328, p. 169–179.

Kilinc, I.A., and Burnham, C.W., 1972, Partitioning of chloride between a silicate melt and coexisting aqueous phase from 2 to 8 kbar: Economic Geology and the Bulletin of the Society of Economic Geologists, v. 67, p. 231, doi:10.2113/gsecongeo.67.2.231.

Lozano-Santa Cruz, R., Verma, S.P., Girón, P., Velasco, F., Morán, D., Viera, F., and Chávez, G., 1995, Calibración preliminar de fluorescencia de rayos X para análisis cuantitativo de elementos mayores en rocas ígneas: Actas INAGEQ, v. 1, p. 203–208.

Ludwig, K.L, 2008, Isoplot/Ex v.3.60. A geochronological toolkit for Microsoft Excel: Berkeley Geochronology Center Special Publication No. 4, reviewed August 26, 2008, 77 p.

Ludwig, K.L., and Mundil, R., 2002, Extracting reliable U-Pb ages and errors from complex populations of zircons from Phanerozoic tuffs: Journal of Conference Abstracts, 12th Goldschmidt Conference, A-463.

Maniar, P.D., and Piccoli, P.M., 1989, Tectonic discrimination of granitoids: Geological Society of America Bulletin, v. 101, p. 635, doi:10.1130/0016-7606(1989)101<0635:TDOG>2.3.CO;2.

Martini, M., 2008, Estratigrafía, deformación y magmatismo de la región comprendida entre Huetamo y Zihuatanejo (Michoacán, Guerrero): Implicaciones para la evolución tectónica del sur de México durante el Cretácico y el Terciario temprano [Ph.D. thesis]: Mexico City, Universidad Nacional Autónoma de México, 256 p.

Martini, M., Ferrari, L., López-Martínez, M., Cerca-Martínez, M., Valencia, V.A., and Serrano-Durán, L., 2009, Cretaceous–Eocene magmatism and Laramide deformation in southwestern Mexico: No role for terrane accretion, *in* Kay, S.M., Ramos, V.A., and Dickinson, W.R., eds., Backbone of the Americas: Shallow Subduction, Plateau Uplift, and Ridge and Terrane Collision: Geological Society of America Memoir 204, p. 151–182, doi: 10.1130/2009.1204(07).

Martiny, B., Martínez-Serrano, R., Morán-Zenteno, D.J., Macías-Romo, C., and Ayuso, R.A., 2000, Stratigraphy, geochemistry, and tectonic significance of the Oligocene magmatic rocks of western Oaxaca, southern Mexico: Tectonophysics, v. 318, p. 71–98, doi:10.1016/S0040-1951(99)00307-8.

McDonough, W.F., and Sun, S.-s., 1995, The composition of the Earth: Chemical Geology, v. 120, p. 223–253, doi:10.1016/0009-2541(94)00140-4.

Meschede, M., Frisch, W., Herrmann, U., and Ratschbacher, L., 1996, Stress transmission across an active plate boundary: An example from southern Mexico: Tectonophysics, v. 266, p. 81–100, doi:10.1016/S0040-1951(96)00184-9.

Meza-Figueroa, D., Valencia-Moreno, M., Valencia, V., Ochoa-Landín, L., Pérez-Segura, E., and Díaz-Delgado, C., 2003, Major and trace element geochemistry and $^{40}Ar/^{39}Ar$ geochronology of Laramide plutonic rocks associated with gold-bearing Fe skarn deposits in Guerrero state, southern Mexico: Journal of South American Earth Sciences, v. 16, p. 205–217, doi:10.1016/S0895-9811(03)00068-3.

Morán-Zenteno, D.J., 1992, Investigaciones isotópicas de Rb-Sr y Sm-Nd en rocas cristalinas de la región de Tierra Colorada–Acapulco–Cruz Grande, Estado de Guerrero [Ph.D. thesis]: Universidad Nacional Autónoma de México, UACPyP del CCH, Instituto de Geofísica, 186 p.

Morán-Zenteno, D.J., Corona-Chávez, P., and Tolson, G., 1996, Uplift and subduction erosion in southwestern Mexico since the Oligocene: Pluton geobarometry constraints: Earth and Planetary Science Letters, v. 141, p. 51–65, doi:10.1016/0012-821X(96)00067-2.

Morán-Zenteno, D.J., Tolson, G., Martínez-Serrano, R., Martiny, B., Schaaf, P., Silva-Romo, G., Macías-Romo, Alba-Aldave, L., Hernández-Bernal, M.S., and Solís-Pichardo, G., 1999, Tertiary arc-magmatism of the Sierra Madre del Sur, Mexico, and its transition to the volcanic activity of the Trans-Mexican Volcanic Belt: Journal of South American Earth Sciences, v. 12, p. 513–535, doi:10.1016/S0895-9811(99)00036-X.

Morán-Zenteno, D.J., Cerca, M., and Keppie, J.D., 2005, La evolución tectónica y magmática cenozoica del suroeste de México: Avances y problemas de interpretación: Boletín de la Sociedad Geológica Mexicana Volumen Conmemorativo del Centenario Temas Selectos de la Geología Mexicana Tomo LVII, no. 3, p. 319–341.

Morán-Zenteno, D.J., Cerca, M., and Keppie, J.D., 2007, The Cenozoic tectonic and magmatic evolution of southwestern México: Advances and problems of interpretation, *in* Alaniz-Álvarez, S.A., and Nieto-Samaniego, Á.F., eds., Geology of México: Celebrating the Centenary of the Geological Society of México: Geological Society of America Special Paper 422, p. 71–91, doi: 10.1130/2007.2422(03).

Mori, L., Gómez-Tuena, A., Cai, Y., and Goldstein, S.L., 2007, Effects of prolonged flat subduction on the Miocene magmatic record of the central Trans-Mexican Volcanic Belt: Chemical Geology, v. 244, p. 452–473, doi:10.1016/j.chemgeo.2007.07.002.

Nieto-Samaniego, A.F., Alaníz-Álvarez, S., Silva-Romo, G., Equiza-Castro, M.H., and Mendoza-Rosales, C.C., 2006, Latest Cretaceous to Miocene deformation events in the eastern Sierra Madre del Sur, Mexico, inferred from the geometry and age of major structures: Geological Society of America Bulletin, v. 118, p. 238–252, doi:10.1130/B25730.1.

Nohl, U., and Sarbas, B., 1999, GEOROC, the MPI Geochemical Rock Database: Introduction of the Web Interface: AGU Fall Meeting, Eos (Transactions, American Geophysical Union).

Ortega-Gutiérrez, F., Sed1ock, R.L., and Speed, R.C., 1994, Phanerozoic tectonic evolution of Mexico, *in* Speed, R.C., ed., Phanerozoic Evolution of North American Continent-Ocean Transitions: Geological Society of America, Decade of North American Geology Summary Volume to accompany the DNAG Continent-Ocean Transects Series, p. 265–306.

Ortega-Gutiérrez, F., Elías-Herrera, M., Reyes-Salas, M., Macías-Romo, C., and López, R., 1999, Late Ordovician–Early Silurian continental collisional orogeny in southern Mexico and its bearing on Gondwana-Laurentia connections: Geology, v. 27, p. 719–722, doi:10.1130/0091-7613(1999)027<0719:LOESCC>2.3.CO;2.

Pearce, J., Harris, N.B., and Tindle, A.G., 1984, Trace element discrimination diagrams for the tectonic interpretation of granitic rocks: Journal of Petrology, v. 25, p. 956–983.

Pérez-Gutiérrez, R., Solari, L.A., Gómez-Tuena, A., and Martens, U., 2009, Mesozoic geologic evolution of the Xolapa migmatitic complex north of Acapulco, southern Mexico: Implications for paleogeographic reconstructions: Revista Mexicana de Ciencias Geológicas, v. 26, p. 201–221.

Petford, N., Cruden, A.R., McCaffrey, K.J.W., and Vigneresse, J., 2000, Granite magma formation, transport and emplacement in the Earth's crust: Nature, v. 408, p. 669–673, doi:10.1038/35047000.

Pupin, J.P., 1980, Zircon and granite petrology: Contributions to Mineralogy and Petrology, v. 73, p. 207–220, doi:10.1007/BF00381441.

Pupin, J.P., 1988, Granites as indicators in paleogeodynamics: Rendiconti della Società Italiana di Mineralogia e Petrologia, v. 43, p. 237–262.

Rämö, O.T. and Haapala, I., 1996, Rapakivi granite magmatism: A global review with emphasis on petrogenesis, *in* Demaiffe, D., ed., Petrology and geochemistry of magmatic suites of rocks in the continental and oceanic crusts. A volume dedicated to Professor Jean Michot: Université Libre de Bruxelles, Royal Museum for Central Africa, p. 177–200.

Schaaf, P., 1990, Isotopengeochemisehe Untersuchungen an granitoiden Gesteimen eines activen Kontinentalsandes: Alter un Herkunft der Tiefengesteinskomplexe an der Pazifikküste Mexikos zwischen Puerto Vallarta und Acapulco [Ph.D. thesis]: Munich, Univ. München, 202 p.

Schaaf, P., Morán-Zenteno, D., Hernández-Bernal, M.S., Solís-Pichardo, G., Tolson, G., and Köhler, H., 1995, Paleogene continental margin truncation in southwestern Mexico: Geochronological evidence: Tectonics, v. 14, p. 1339–1350, doi:10.1029/95TC01928.

Schaaf, P., Böhnel, H., and Pérez-Venzor, J.A., 2000, Pre-Miocene palaeogeography of the Los Cabos block, Baja California Sur: Geochronological and palaeomagnetic constraints: Tectonophysics, v. 318, p. 53–69, doi:10.1016/S0040-1951(99)00306-6.

Schaaf, P., Stimac, J., Siebe, C., and Macías, J.L., 2005, Geochemical evidence for mantle origin and crustal processes in volcanic rocks from Popocatépetl and surrounding monogenetic volcanoes, central Mexico: Journal of Petrology, v. 46, p. 1243–1282, doi:10.1093/petrology/egi015.

Schmidt, M.W., 1992, Amphibole composition in tonalite as a function of pressure: An experimental calibration of the Al-in-hornblende barometer: Contributions to Mineralogy and Petrology, v. 110, p. 304–310, doi:10.1007/BF00310745.

Sedlock, R.L., Ortega-Gutiérrez, F., and Speed, R.C., 1993, Tectonoestratigraphic Terranes and Tectonic Evolution of Mexico: Geological Society of America Special Paper 278, 153 p.

Snow, E., and Kidman, S., 1991, Effect of fluorine on solid-state alkali interdiffusion rates in feldspar: Nature, v. 349, p. 231–233, doi:10.1038/349231a0.

Solari, L.A., Keppie, J.D., Ortega-Gutíerrez, F., Cameron, K.L., López, R., and Hames, W.E., 2003, 990 and 110 Ma Grenvillian tectonothermal events in the northern Oaxacan Complex, southern Mexico: Roots of an orogen: Tectonophysics, v. 365, p. 257–282, doi:10.1016/S0040-1951(03)00025-8.

Solari, L.A., Keppie, J.D., Ortega, G.F., Cameron, K.L., and López, R., 2004, ~990 Ma peak granulitic metamorphism and amalgamation of Oaxaquia Mexico: U-Pb zircon geochronological and common Pb isotopic data: Revista Mexicana de Ciencias Geológicas, v. 21, p. 212–215.

Solari, L.A., Torres de León, R., Hernández-Pineda, G., Solé, J., Solís-Pichardo, G., and Hernández-Treviño, T., 2007, Tectonic significance of Cretaceous–Tertiary magmatic and structural evolution of the northern margin of the Xolapa Complex: Tierra Colorada area, southern Mexico: Geological Society of America Bulletin, v. 119, p. 1265–1279, doi:10.1130/B26023.1.

Solari, L.A., Gómez-Tuena, A., Bernal, J.P., Pérez-Arvizu, O., and Tanner, M., 2010, U-Pb zircon geochronology by an integrated LA-ICPMS microanalytical workstation: Achievements in precision and accuracy: Geostandards and Geoanalytical Research, v. 34, p. 5–18, doi:10.1111/j.1751-908X.2009.00027.x.

Stimac, J.A., and Wark, D.A., 1992, Plagioclase mantles on sanidine in silicic lavas, Clear Lake, California: Implications for the origin of rapakivi texture: Geological Society of America Bulletin, v. 104, p. 728, doi:10.1130/0016-7606(1992)104<0728:PMOSIS>2.3.CO;2.

Straub, S.M., and Layne, G.D., 2003, The systematics of chlorine, fluorine, and water in Izu arc front volcanic rocks: Implications for volatile recycling in subduction zones: Geochimica et Cosmochimica Acta, v. 67, p. 4179–4203, doi:10.1016/S0016-7037(03)00307-7.

Sun, S.-s., and McDonough, M.F., 1989, Chemical and isotopic systematics of oceanic basalts: Implications for mantle composition and processes: The Geological Society of London Special Publication 42, p. 313–345.

Talavera-Mendoza, O., Ruíz, J., Gehrels, G.E., Valencia, V., and Centeno-García, E., 2007, Detrital zircon U/Pb geochronology of southern Guerrero and western Mixteca arc successions (southern Mexico): New insights for the tectonic evolution of southwestern North America during the late Mesozoic: Geological Society of America Bulletin, v. 119, p. 1052–1065, doi:10.1130/B26016.1.

Valencia, V.A., Ducea, M., Talavera-Mendoza, O., Gehrels, G., Ruiz, J., and Shoemaker, S., 2009, U-Pb geochronology of granitoids in the north-western boundary of the Xolapa Terrane: Revista Mexicana de Ciencias Geológicas, v. 26, p. 189–200.

Vigneresse, J.L., 1995a, Control of granite emplacement by regional deformation: Tectonophysics, v. 249, p. 173–186, doi:10.1016/0040-1951(95)00004-7.

Vigneresse, J.L., 1995b, Crustal regime of deformation and ascent of granitic magma: Tectonophysics, v. 249, p. 187–202.

Walker, J.D., Bowers, T.D., Black, R.A., Glazner, A.F., Farmer, G. L., and Carlson, R.W., 2006, A geochemical database for western North American volcanic and intrusive rocks (NAVDAT), *in* Sinha, A.K., ed., Geoinformatics: Data to Knowledge: Geological Society of America Special Paper 397, p. 61–71, doi: 10.1130/2006.2397(05).

Whalen, J.B., Currie, K.L., and Chappell, B.W., 1987, A-type granites: geochemical characteristics, discrimination and petrogenesis: Contributions to Mineralogy and Petrology, v. 95, p. 407–419, doi:10.1007/BF00402202.

Wiedenbeck, M., Alle, P., Corfu, F., Griffin, W.L., Meier, M., Oberli, F., Von Quadt, A., Roddick, J.C., and Spiegel, W., 1995, Three natural zircon standards for U-Th-Pb, Lu-Hf, trace element and REE analyses: Geostandards Newsletter, v. 19, p. 1–23, doi:10.1111/j.1751-908X.1995.tb00147.x.

Wilson, M., 1989, Igneous Petrogenesis: A Global Tectonic Approach: Dordrecht, The Netherlands, Springer, 466 p.

Manuscript Received 2 August 2011
Revised Manuscript Received 2 September 2011
Manuscript Accepted 3 September 2011